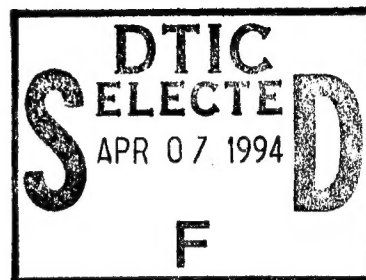PL-TR-94-2299

INVESTIGATION OF THE TRANSPORTABILITY OF THE *P/S* RATIO DISCRIMINANT TO DIFFERENT TECTONIC REGIONS

Douglas Baumgardt
Zoltan Der

ENSCO, Inc.
Signal Analysis and Systems Division
5400 Port Royal Road
Springfield, Virginia 22152-2301

DTIC
SELECTED
APR 07 1994
S F D

6 December 1994

Scientific Report No. 1

Approved for public release; distribution unlimited

PHILLIPS LABORATORY
Directorate of Geophysics
AIR FORCE MATERIEL COMMAND
HANSCOM AFB, MA 01731-3010

19950405 043
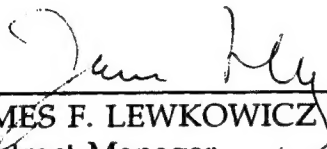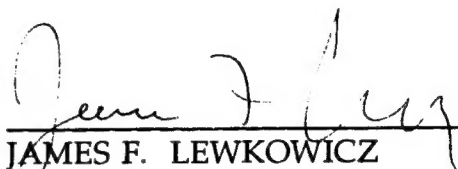
SPONSORED BY
Advanced Research Projects Agency (DoD)
Nuclear Monitoring Research Office
ARPA ORDER No. A-128

MONITORED BY
Phillips Laboratory
CONTRACT No. F19628-93-C-0103

This technical report has been reviewed and is approved for publication.

JAMES F. LEWKOWICZ
Contract Manager
Earth Sciences Division

JAMES F. LEWKOWICZ
Director
Earth Sciences Division

REPORT DOCUMENTATION PAGE

Form Approved
OMB No. 0704-0188

1. AGENCY USE ONLY (Leave blank)	2. REPORT DATE 6 December 1994	3. REPORT TYPE AND DATES COVERED Scientific #1

4. TITLE AND SUBTITLE

Investigation of the Transportability of the P/S Ratio Discriminant to Different Tectonic Regions

5. FUNDING NUMBERS
PE 62301E
PR NM 93 TA GM WU AC
Contract F19628-93-C-0103

6. AUTHOR(S)
Douglas Baumgardt
Zoltan Der

7. PERFORMING ORGANIZATION NAME(S) AND ADDRESS(ES)

ENSCO, Inc.
Signal Analysis and Systems Division
5400 Port Royal Road
Springfield, VA 22151-2301

8. PERFORMING ORGANIZATION REPORT NUMBER

9. SPONSORING/MONITORING AGENCY NAME(S) AND ADDRESS(ES)

Phillips Laboratory
29 Randolph Road
Hanscom AFB, MA 01731-3010

Contract Manager: James Lewkowicz/GPEH

10. SPONSORING/MONITORING AGENCY REPORT NUMBER

PL-TR-94-2299

11. SUPPLEMENTARY NOTES

12a. DISTRIBUTION/AVAILABILITY STATEMENT

Approved for public release; distribution unlimited

12b. DISTRIBUTION CODE

13. ABSTRACT (Maximum 200 words)

We have developed, analyzed, and contrasted two methods for correcting measurements of Pn/Sn and Pn/Lg ratio for distance in the Scandinavian shield, the first based on an earlier detection study of Sereno (1991) and the second method has been developed specifically for regions of sparse station coverage. Both methods provide smooth distance correction curves which can correct amplitude ratio measurements to a standard distance. However, we have observed large scatter in the observations of Pn/Sn and Pn/Lg ratios as a function of distance, and the distance correction curves are not well constrained. Crustal cross sections of propagation paths in three different tectonic regions, have been derived from on-line GIS databases, and we have found approximate correlations of high-frequency Pn/Lg amplitude ratio with the crustal parameters of average elevation, average depth to basement (sediment thickness), and gradients in these parameters. Using these correlations and comparing Pn/Lg ratio measurements of a Chinese nuclear explosion with blasts in eastern Europe and Scandinavia, we find that Pn/Lg ratios in the Scandinavian shield need to be decreased by nearly 0.8 log units when comparing them to events in tectonically active regions like China. Similar analyses can be used for transporting discriminants in the future to other tectonically active regions, such as the Middle East.

14. SUBJECT TERMS			15. NUMBER OF PAGES 76
Discrimination	Tectonics	Earthquakes	
Seismology	Geology	Mine Blasts	
Regional	Propagation	Nuclear explosions	16. PRICE CODE
	Testban Treaty		

17. SECURITY CLASSIFICATION OF REPORT Unclassified	18. SECURITY CLASSIFICATION OF THIS PAGE Unclassified	19. SECURITY CLASSIFICATION OF ABSTRACT Unclassified	20. LIMITATION OF ABSTRACT SAR

NSN 7540-01-280-5500

Standard Form 298 (Rev. 2-89)
Prescribed by ANSI Std. Z39-18
298-102

TABLE OF CONTENTS

1.0 INTRODUCTION

1.1 Development of the *P/S* Ratio Discriminant

The regional *P/S* amplitude ratio has long been investigated as a possible discriminant between explosions and earthquakes, because intuitively, earthquakes being shear, dislocation type sources should produce more shear-wave energy than explosions (Pomeroy et al, 1981). Thus, *P/S* ratios should be lower for earthquakes than for explosions. Early studies in the 1970's and early 1980's demonstrated the potential of the discriminant (e.g., Blandford et al, 1981) for separating explosions and earthquakes. However, studies of the *P/Lg* ratio discriminant at low frequencies by Nuttli (1981), Bennett and Murphy (1986), and Taylor et al (1989) found significant overlap in the earthquake and explosion populations for events in Eurasia and in Western United States.

Bennett et al (1989) demonstrated improved separation of nuclear explosions and earthquakes on the basis of high frequency *S/P* ratios. Dysart and Pulli (1990) showed the same trend for mine blasts and explosions in Scandinavia recorded at the NORESS array. However, in both studies, the earthquake and explosion groups were not in the same geographic region and propagation-path differences may have biased the discrimination results. Baumgardt and Young (1990) studied mine blasts and earthquakes which were in the same region in Scandinavia and showed that mine blasts have significantly higher *Pn/Lg* ratios at high frequency than earthquakes. Interestingly, they showed that the discrimination was due to explosions having higher *Pn* energy than to earthquakes, whereas their *Lg* levels were about the same. Kim et al (1993) also demonstrated the success of this discriminant at high frequencies for quarry blasts and earthquakes in Eastern U.S.

1.2 The Discriminant Transportability Problem

Discrimination research has always been burdened by the need to understand the effects of propagation path structure on high-frequency seismic waveforms. To remove the effects of propagation path bias, earthquakes and explosions in the same geographic region have been sought (e.g., Murphy and Bennett, 1982; Bennett and Murphy, 1988; Baumgardt and Young, 1990). In other studies, the various kinds of sources (nuclear explosions, earthquakes, mine blasts) have been in entirely different regions (Taylor et al, 1988, 1989; Pulli and Dysart, 1990) which leaves open the question of how much differences in propagation-paths biased the discrimination results.

Lynnes and Baumstark (1991), for example, demonstrated propagation path effects on P/S amplitude ratio discriminants and Lg spectral ratio discriminants for numerous events in North America that caused poor discrimination results. One may also encounter positive but false discrimination results because of effects of propagation path if explosions and earthquakes occur in different regions which have different propagation path effects.

A good example of how propagation path effects may bias discriminants was the recent experiment to identify a seismic event near Novaya Zemlya, which occurred on December 31, 1992 (Ryall, 1993). Initially, all of the investigators who participated, including ENSCO (Baumgardt, 1993b), identified the event as mine blast, based mainly on analysis of high-frequency Pn/Sn. Comparison of the measured ratios with reference events placed the 31 December 1992 event in the Kola mine blast population. Fisk et al (1993) determined that this conclusion was statistically valid, based on analysis of the same features. However, the 31 December 1992 event was in a different region than the Kola blasts and was much farther away from the ARCESS array. Baumgardt (1993b) concluded that this event was an earthquake, based on these noted propagation path differences and a relative scaling argument using an earlier earthquake recorded at NORESS.

This example may be typical of a future CTBT or NPT monitoring problem, where an event of unknown identity occurs in a region where there has been little or no seismicity or a limited seismological record available. To try to characterize such events, which we call "special events," feature comparisons must be made between the unknown event and known events in other parts of the world. This "discriminant transportability" problem requires the monitoring system to account for such propagation path biasing effects, to correct for them, or to use discriminants which are insensitive to such biasing effects.

There are two problems associated with transporting the P/S ratio discriminants (Pn/Sn, Pn/Lg) from one region to another.

(1)   These amplitude ratios depend on distance of propagation, even in the same tectonic region, because the Pn and Lg amplitudes attenuate at different rates with distance. The same is also true of the Pn/Sn ratio, used in regions where Lg waves are blocked, such as for events at Novaya Zemlya recorded at ARCESS (Baumgardt, 1993). Thus, classifying seismic events with reference or training events at different distances will require some kind of path correction for distance which accounts for the differential attenuation of Pn and Sn or Lg.

(2) Pn/Lg ratios can vary significantly due to partial or complete blockages of Lg, which Baumgardt (1990) showed could be caused by sudden variations in shallow crustal structure, such as when Lg waves propagate across sedimentary basins. Lg "blockages" can cause sharp increases in the Pn/Lg

ratio and could make earthquakes have "explosion-like" high ratios which could cause them to be misclassified if the blockages are not identified.

This report presents the results of a study which addresses these two problems associated with transporting regional discriminants. First, to transport P/S amplitude ratios from one distance to another in the same tectonic region, we present a technique of using station pairs at different separation distances to determine amplitude ratios as a function of distance. The second problem of correcting for possible blockage effects in the upper crust when transporting discriminants across tectonic boundaries requires knowledge of the crustal structure. To correct for this kind of blockage, we have investigated correlations between Pn/Lg amplitude ratios with crustal parameters derived from GIS databases (Fielding et al, 1992) using techniques similar to those of Zhang and Lay (1993a,b), and Zhang et al (1994).

Section 2.0 of this report describes the method for measuring regional P/S ratios, used in the data analysis for this study. Section 3.0 discusses two methods for correcting regional P/S ratios for distance, one based on a regional-phase detection study of Sereno (1991) and a new method we have developed applicable to regions where station coverage is sparse. Section 4.0 addresses the more difficult problem of transporting the Pn/Lg ratio discriminant to a new region for which there is limited historical seismic data. Following on the work of Baumgardt (1990) and Zhang et al (1994), we investigate a method of using crustal cross sections between a source and station to calibrate Pn/Lg ratios. Section 5.0 summarizes the conclusions and makes recommendations for an approach for transporting the regional P/S ratio discriminant from one region to another.

2.0 *P/S* MEASUREMENT APPROACH

Following on the research of Baumgardt and Young (1990), ENSCO implemented the regional *P/S* ratio discriminant in the Intelligent Seismic Event Identification System (ISEIS) (Baumgardt et al. 1991). The system was specifically designed to exploit multichannel high-frequency data recorded at the regional arrays NORESS, ARCESS, FINESA, and GERESS. For this study, we rely on measurements of *P/S* ratios made in the ISEIS system on high-frequency data from both arrays and single stations.

ISEIS measures several varieties of *P/S* ratios on **incoherent beams** computed from individual traces recorded at the regional arrays. An example of a bandpass filtered trace recorded at the array ARCESS and its corresponding **log-RMS** incoherent beam are shown in Figure 1. Given a set of seismogram time-series amplitudes at time i on array channel $A_j(ti, \Delta f)$, which have been prefiltered in the band Δf, the log-RMS incoherent beam value at time τ is computed as follows:

$$A_{RMS}^{\log}(\tau; \Delta f) = \frac{1}{N} \sum_{j=1}^{N} \log_{10} \left[\frac{1}{K} \sqrt{\sum_{ti=t1}^{t2} A^2_j(ti; \Delta f)} \right], \qquad (1)$$

where K is the number of time points in time window from $t1$ to $t2$, N is the number of channels in the array, and $\tau = t1 + \left(\frac{t2 - t1}{2} \right)$. These measures are made for adjacent time windows shifted down the trace, and when plotted as a function of the window time, τ, the result is an envelope of the trace, as shown in Figure 1. We have experimented with a number of different kinds of incoherent beams and have found that the log RMS display gives the most informative view of the regional waveform shape. By averaging log RMS amplitude estimates over the array, local receiver function effects at the individual array sites are averaged out and a smoothed estimate of the seismogram shape results. In the case of single-channel, or three-component data, the same time-average calculations can be done for the single channels.

ISEIS measures these incoherent beams for seismograms prefiltered in several frequency bands using 6th order Butterworth recursive bandpass filters. For high frequency data at the NORESS-type arrays, which are sampled at 40 cps, the filter bands are 0.5-2.0 Hz (for Rg detection), 2-4 Hz, 2.5-4.5 Hz, 3-5 Hz, 4-6 Hz, 5-7 Hz, 6-8 Hz, 8-10 Hz, and 8-16 Hz. These pre-filters can be modified for other sampling rates. For example, to process three-component Chinese Digital Seismic Network (CDSN) on the midband channels (*bz, bn, be*), filters designed

4

(b)

(a)
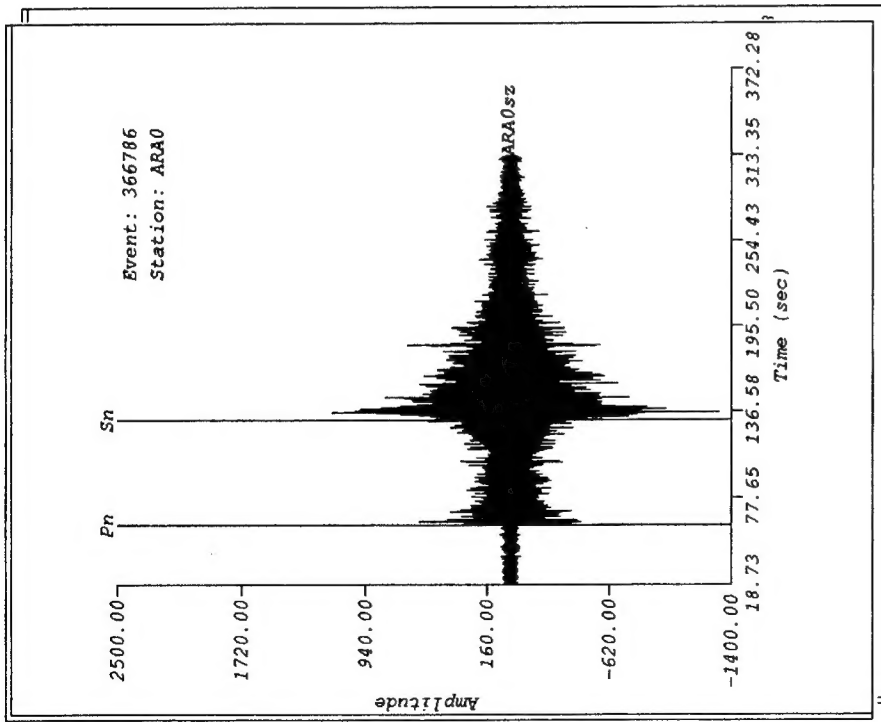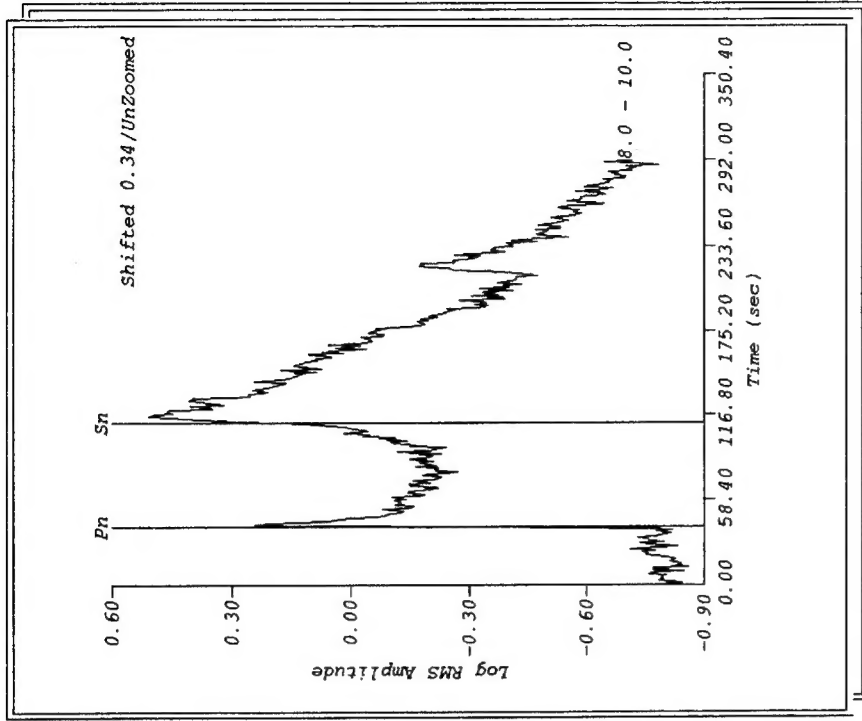
Figure 1: Time domain amplitude measurements are made on envelope traces called incoherent beams (IBEAMS), as shown for a mine blast recorded at ARCESS. (a) ARCESS center element (ARA0) bandpass filtered in the 8-16 Hz band. Time picks made by the analyst are shown. Time traces are bandpass filtered in 9 bands. (b) Envelope traces are computed from the filtered seismogram by averaging the rms amplitudes in 1 second windows shifted down the trace. For arrays, IBEAMs are computed from averages of the envelopes across the array. For single stations, IBEAMS are the envelopes of the single traces.

for 20 cps sampling rates are provided but without the 8-16 Hz filter since this band exceeds the Nyquist frequency of 10 Hz.

Figure 2 shows an example of the entire suite of bandlimited incoherent beams computed for an ARCESS recording of a Kola Peninsula mine blast. Each of the incoherent beams have been shifted for viewing purposes. These displays have been very useful for analyzing the frequency trends of regional seismogram shapes and for characterizing various regional phases as a function of frequency.

After computing the incoherent beams, the next step is to estimate the regional phase amplitudes off the incoherent beams. Regional phase picks, as shown in Figure 1, are noted on the incoherent beams. These phase picks generally come from measurements made in the Intelligent Monitoring System (Bache et al, 1990) which are later reviewed by the analyst. We also review the phase picks in the ISEIS system and make corrections, if necessary. Amplitude measures are then made in time windows on the incoherent beams beginning at these phase picks. The time windows are either set automatically, using assumed group velocities, or interactively by the analyst. An example of the measurement of the amplitude of a *Pn* phase in the 8 to 10 Hz band is shown in Figure 3. Two kinds of amplitudes are measured: *Amax*, which is the maximum amplitude in the incoherent beam time window, and *Aavg*, which is the average time in the window. These estimates are made for all the associated phases on all bandlimited incoherent beams and are stored in the Oracle database.

Finally, amplitude ratio measures for a regional *P* and *S* phase are made on all unique combinations in each frequency band:

$$R^{avg}(f) = \frac{A_{avg}^{P}(f)}{A_{avg}^{S}(f)} \tag{2}$$

for the average amplitude estimates and

$$R^{max}(f) = \frac{A_{max}^{P}(f)}{A_{max}^{S}(f)} \tag{3}$$

for the maximum amplitude estimates. Note that ratios are made in the same frequency bands. All these ratios are computed for all unique combinations of phases in all frequency bands available and the results stored in the Oracle database.
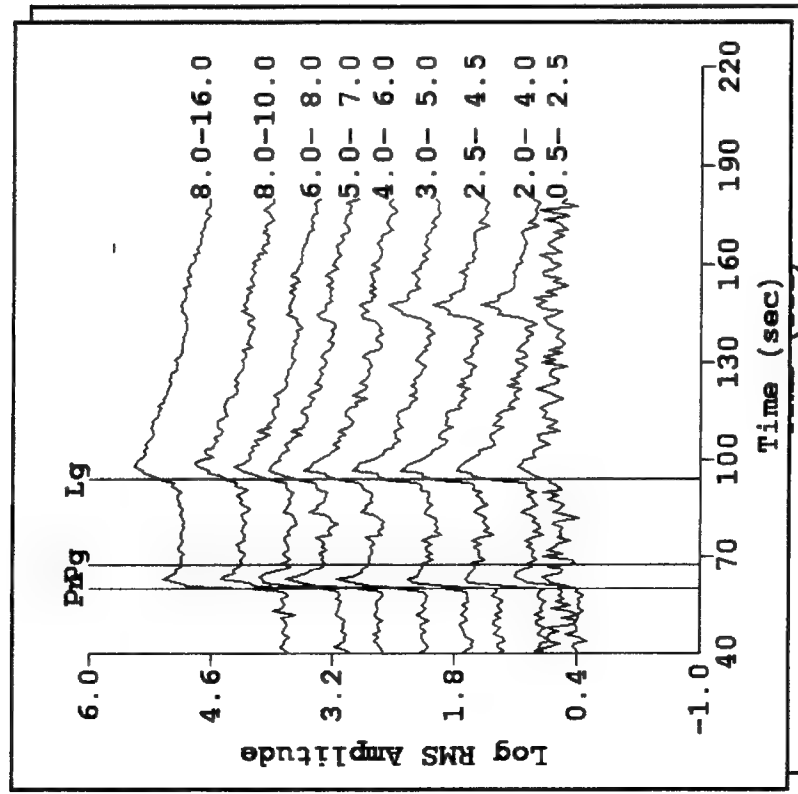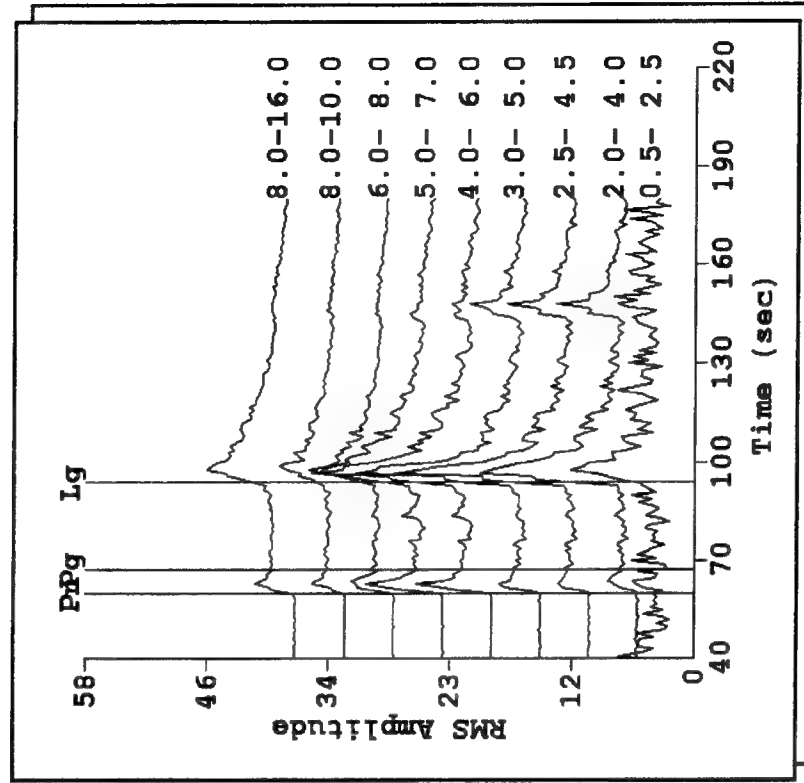
Figure 2: Examples of incoherent beams (IBEAMS) in 9 frequency bands for an event in the Kiruna mine of northern Sweden. (a) log RMS beams, (b) unlogged RMS beams. Amplitude ratios are measured on all IBEAMS in all frequency bands. Waveform phase picks made by the analyst on seismograms are shown at the corresponding times on the incoherent beams.

7
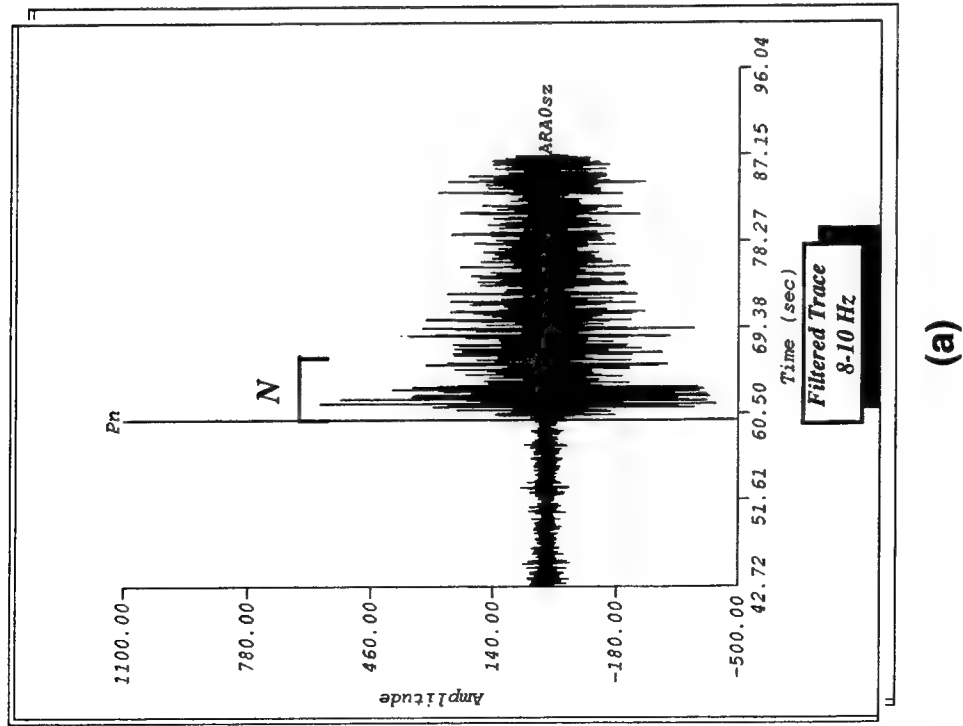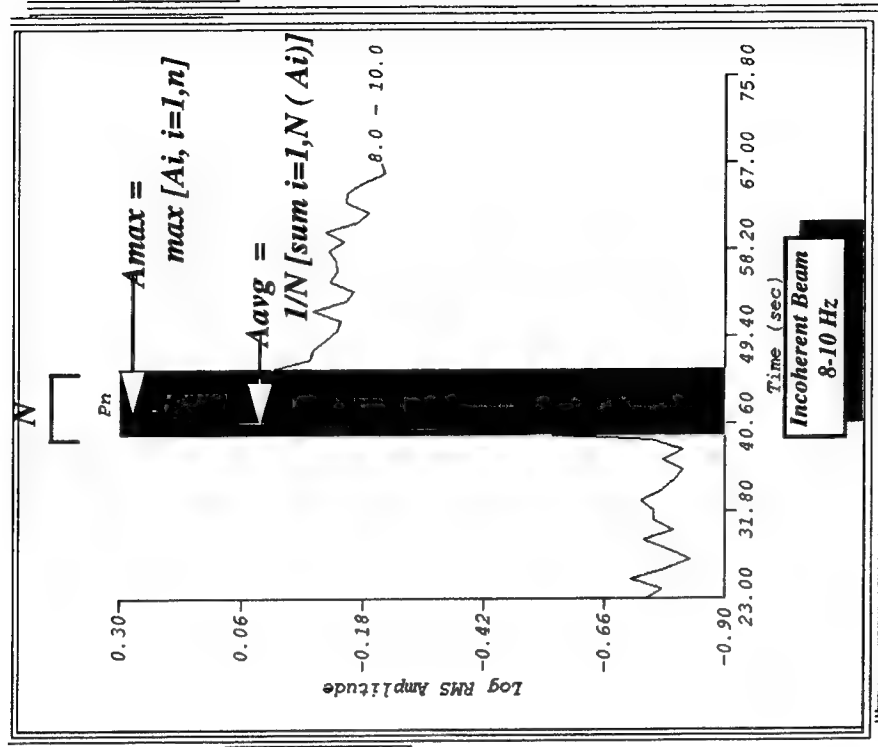
Figure 3: (a) Amplitudes are measured from incoherent beams on "phase selections", or time windows of specified length (*N*), starting at the time of the picked phase onset. (b) Both maximum and average estimates of IBEAM amplitude are made. Maximum amplitudes are usually best since they are less dependent on assumed window length, *N*.

8

Measurements of this kind have been made for many examples of mine explosions, nuclear explosions, earthquakes, and quarry blasts. A variety of scatter plot displays are provided for displaying the results in comparison with the CURRENT EVENT, which is a user selected special event which needs to be characterized. Amplitude ratios can be plotted as a function of geographic region, distance, frequency, magnitude, depth of focus (if known), and signal-to-noise ratio. For the latter display, the same amplitude measures are made on background noise and signal-to-noise ratios are computed for all phases and stored to the database. Examples of these kinds of plots will be shown later in this report.

3.0 DISTANCE DEPENDENCE OF THE *P/S* RATIO DISCRIMINANT

Previous studies of amplitude changes of regional phases as a function of distance (e.g., Chun et al, 1987; Chun, et al, 1989; Sereno, 1991) have clearly shown that the amplitudes of regional *P* and *S* phases will not decay at the same rate. Most of these studies have assumed that the amplitudes of individual regional phases decay with distance due to anelastic attenuation and geometric spreading, both of which will be different for *P* and *S*. Thus, we might expect that curves of *P/S* amplitude ratios versus distance, for events in regions where anelastic attenuation and geometric spreading effects are laterally homogeneous, to be relatively smooth and systematic. However, Kennett (1993) studied the distance dependence of *Pn*, *Sn*, and *Lg* amplitudes from a single explosion source, using data from the Fennolora long-range refraction study in Sweden, and found significant scatter in *Pn/Sn* and *Pn/Lg* amplitude ratios as a function of distance. He argued that the complexities of *Pn* and *Sn* interactions in the crust and upper mantle cause complex variations in amplitudes of these phases as a function of distance. Thus, *Pn/Sn* and *Pn/Lg* amplitude ratios may not be predictable from simple parametric expressions for anelastic attenuation and geometric spreading.

In this section, we address the question of correcting *Pn/Sn* and *Pn/Lg* amplitude ratios for distance by testing the hypothesis that simple, parametric correction curves can be utilized. Specifically, we compare two different methods for correcting amplitude ratios for distance-dependent attenuation. The first one, based on the multiple-event amplitude distance corrections determined by Sereno (1991), was recently used by Fisk (1994) in a reinterpretation of the *Pn/Sn* amplitude ratio discriminant applied to the December 31, 1992 Novaya Zemlya event. The second method is a new approach developed specifically for regions where there are only a few stations separated by large distances. In this approach, we derive a new set of *Pn/Sn* and *Pn/Lg* amplitude-ratio distance-correction curves for Scandinavia by directly fitting the amplitude-ratio measurements themselves, rather than the individual amplitudes, to simple distance-dependent relations. We then show how well these curves can correct amplitude ratios for distance. Note that both these approaches assume that the measurements are made for events at different distances in the same geographic-tectonic region.

3.1 The *Sereno* Multiple Event Distance Correction Method

Recently, Fisk (1994) utilized the amplitude-distance parameters of Sereno (1991) to correct *Pn/Sn* amplitude ratios for distance. The method apparently resolved the ambiguity of the

Pn/Sn ratios for the December 31, 1992 Novaya Zemlya event in that, after correction, the ratios were more consistent with earthquakes. However, Sereno's original study was concerned with detectability of individual regional phases, not with distance corrections of amplitude ratios. He derived relations for the distance decay in different frequency bands of the regional phases *Pn*, *Pg*, *Sn*, and *Lg* using single-array measurements from multiple sources of different magnitudes. The method involves first correcting all the sources which have different magnitudes to the same magnitude by means of a frequency-dependent source scaling. The resulting amplitudes are then fit by regression to a set of analytical expressions. These expressions can then be used to obtain expressions for amplitude ratios between two regional seismic phases, *Ph1* and *Ph2*, as a function of the bandpass-filter center frequency, *f*, in the form

$$\frac{Ph1}{Ph1} = e^{-(a_{01}-a_{02})f}\left(\frac{\Delta}{\Delta_o}\right)^{-(n_{Ph1}-n_{Ph2})} , \tag{4}$$

where $n = a\,f + b$ accounts for geometric spreading and the exponential term accounts for attenuation relative to a reference distance, Δ_o. The coefficients a, b, and ao are based on the individual-phase distance corrections inferred by Sereno (1991), which are shown in Table 1.

TABLE 1:
Amplitude Ratio Distance Correction Parameters
Based on Individual Phase Amplitude Relations of Sereno (1991)

Phase	a_0	a	b
Pn	-0.02	0.072	1.40
Pg	0.11	0.122	2.33
Sn	-0.03	0.125	1.62
Lg	0.19	0.63	0.29

This formulation is useful because it allows amplitude-ratio corrections to be made between any phase pair from one distance to another. Fisk (1994) used the relationship (4) to obtain distance correction for the *Pn/Sn* ratios measured by ISEIS to a standard distance, Δ_0, which is

$$\left(\frac{Pn}{Sn}\right)_{\Delta_o} = \left(\frac{\Delta}{\Delta_o}\right)^{-0.053f-0.22}\left(\frac{Pn}{Sn}\right).$$ (5)

The corresponding relation for Pn/*Lg* ratios is

$$\left(\frac{Pn}{Lg}\right)_{\Delta_o} = \left(\frac{\Delta}{\Delta_o}\right)^{-0.558f+1.11}\left(\frac{Pn}{Lg}\right).$$ (6)

One of the problems of the Sereno (1991) method of computing the distance-dependence of individual phase amplitudes is the use of multiple sources recorded at one station. Given the high variability of P vs. S excitation by various events, the estimation procedure for P/S -ratio distance dependence must be insensitive to variations in relative excitation. Because the sources have different magnitudes, a local-magnitude (Ml) source scaling relationship must be assumed to reduce all events to a common magnitude.

Another possible problem is that the two relations (5) and (6) above imply a completely different distance dependence of the amplitude ratios, depending on frequency. These formulas show that, for a given frequency, the amplitude ratios scale as a constant power of distance relative to a reference distance. Assuming the reference distance and ratio to be 1, the distance dependences for 3 different frequencies, 3, 5, and 9 Hz, are

$f = 3Hz$ $\qquad\qquad\qquad$ $f = 5Hz$ $\qquad\qquad\qquad$ $f = 9Hz$

$\left[\dfrac{Pn}{Sn}\right] = \Delta^{0.379}$ $\qquad\quad$ $\left[\dfrac{Pn}{Sn}\right] = \Delta^{0.485}$ $\qquad\quad$ $\left[\dfrac{Pn}{Sn}\right] = \Delta^{0.697}$

For frequencies less than 14 Hz, the amplitude-ratio (R) vs. distance trend is predicted by these relations to be concave down, relative to a slope 1 line, as shown below:

12
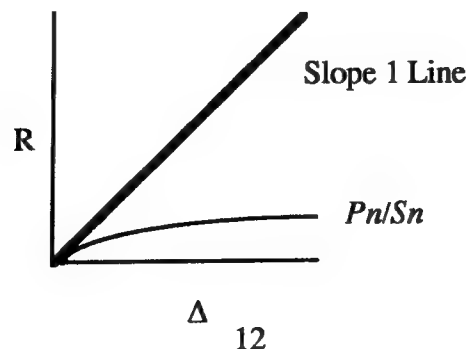
As the frequency approaches 14 Hz, the trend becomes a line of slope 1. Above 14 Hz, the trend is concave up, as shown below:
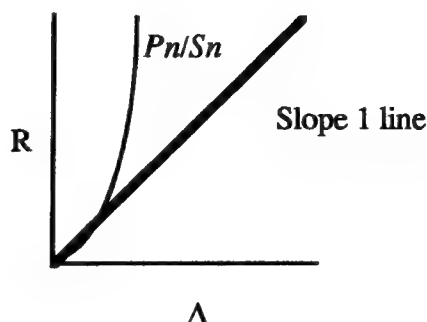
For *Pn/Lg* ratios, the trends at these three frequencies are

$$f = 3Hz \qquad\qquad f = 5Hz \qquad\qquad f = 9Hz$$

$$\left[\frac{Pn}{Lg}\right] = \Delta^{0.564} \qquad\qquad \left[\frac{Pn}{Lg}\right] = \Delta^{1.68} \qquad\qquad \left[\frac{Pn}{Lg}\right] = \Delta^{3.912},$$

Thus, below 3 Hz, the predicted trend for *Pn/Lg* ratios is concave down, whereas above 3 Hz, the trends will be concave up. Thus, for the main frequency band of interest in our discrimination work, which is between 6 and 10 Hz, the Sereno (1990) trends with distance will be concave down for *Pn/Sn* ratios and concave up for *Pn/Lg* ratios. Also, at a frequency of about 9 Hz, the *Pn/Lg* ratio is predicted to have a cubic trend. The differences in the trends for the different frequencies seem extreme.

3.2   The *Exponential* Station Pair Distance Correction Method

A better method of obtaining distance corrections for regional phase amplitudes, which would not require assumptions of source magnitude scaling, would be to compare the P and S amplitudes (or their ratios) of the same events recorded at stations at multiple distances. However, because regional events are small, most of them are usually only recorded at two stations. Also, in many regions, station densities are small and the stations may be widely separated. For example, there are only three regional arrays available for all of Scandinavia, NORESS, ARCESS, and FINESA, which are each separated by over 400 km. This may be typical of a CTBT monitoring scenario where only a small number of alpha stations may be available for a large geographic region. Without using a smaller density network of beta and gamma stations, which may be of

13

lower quality and for which data may not always be available, a method is needed to use the small number of stations to infer distance corrections for amplitude ratios.

We have developed a method to directly infer distance corrections for frequency-dependent amplitude ratios by measuring the ratios for events recorded at pairs of stations which are separated by a range of distances. This method has some similarity to the station-pair method originally developed by Chun et al, (1987) for determining the anelastic attenuation of Lg. However, because we desire corrections for amplitude ratios, rather than absolute amplitudes, the reversed two-station method, developed by Chun et al (1987) to avoid biases caused by differences in station calibration, need not be applied. Thus, we only require one event per station pair, rather than two events needed in the reversed two-station method. The amplitude-ratio distance corrections are computed by a least squares fitting scheme to two or more stations. Thus, for a single event recorded at two stations, we represent the amplitudes of the P ($P1$, $P2$) and $S(S1, S2)$ at the two stations as a simple attenuation-plus-geometric-spreading model:

$$P_1 = A_o \Delta_1^{-n_e} e^{-\frac{\pi f \Delta_1}{Q_p U_p}}$$

$$P_2 = A_o \Delta_2^{-n_e} e^{-\frac{\pi f \Delta_2}{Q_p U_P}}$$

$$(7)$$

for the P waves and

$$S_1 = A_o \Delta_1^{-n_e} e^{-\frac{\pi f \Delta_1}{Q_s U_s}}$$

$$S_2 = A_o \Delta_2^{-n_e} e^{-\frac{\pi f \Delta_2}{Q_s U_s}}$$

$$(8)$$

for the S waves at the two stations. In these expressions, Ao is the initial amplitudes, $\Delta 1$ and $\Delta 2$ the distances of the event from the two stations, Q_P and Q_S are the attenuation quality factors for the P and S waves, respectively, U_P and U_S are the group velocities of the P and S waves, respectively, n_e is the assumed geometric spreading exponent (assumed to be the same for P and S), and f is the frequency of the waves. For the purposes of our analyses, we assume that the frequency f is the center frequency of the 9 filter bands used to compute the incoherent beams on which the amplitudes of the P and S waves are measured.

Figure 4(a) shows a map of the locations of the events which we used for this analysis, that were recorded at two more of four regional arrays, NORESS (NRA0), ARCESS (ARA0), FINESSA (FIA0), and APATITY (APA0). The X's mark the locations of the seismic events which were analyzed. For each of these events, two regional P/S ratios were measured, Pn/Sn and Pn/Lg in the 9 frequency bands. The distances of the events from the different stations ranged from 200 to 2000 km.

For station pairs which recorded single events, we next compute the differences in the logarithms of the ratios at two or more stations as follows:

$$R_1 = \log P_1 - \log S_1 = \pi f \Delta_1 \left[\frac{1}{Q_s U_s} - \frac{1}{Q_p U_p} \right] \log e$$

$$R_2 = \log P_2 - \log S_2 = \pi f \Delta_2 \left[\frac{1}{Q_s U_s} - \frac{1}{Q_p U_p} \right] \log e \tag{9}$$

where $R1$ and $R2$ are the log ratios measured at two stations. The difference in ratios is then:

$$dR = R_2 - R_1 = \pi f \log e \left[\frac{1}{Q_s U_s} - \frac{1}{Q_p U_p} \right] [\Delta_2 - \Delta_1]. \tag{10}$$

Because we have assumed the spreading to be the same for P and S waves and the same initial amplitude, we have a linear relation at a given center frequency f between the difference in ratios and the difference in distances with zero intercept. The gradient of the differential ratios, $Gradient \equiv \nabla = \dfrac{dR}{d\Delta}$, is then integrated over specified distance intervals, $d\Delta$, as follows:

$$A(\Delta_o) = \int_0^{\Delta_o} e^{\nabla(\Delta)} d\Delta. \tag{11}$$

In our analyses, we compute this integral numerically using distance intervals, $d\Delta$, of 10 km. The amplitude ratio at a given distance is then,

$$\frac{P}{S}(\Delta) = 10^{-(Slope)\Delta}, \tag{12}$$

where the *Slope* is written as
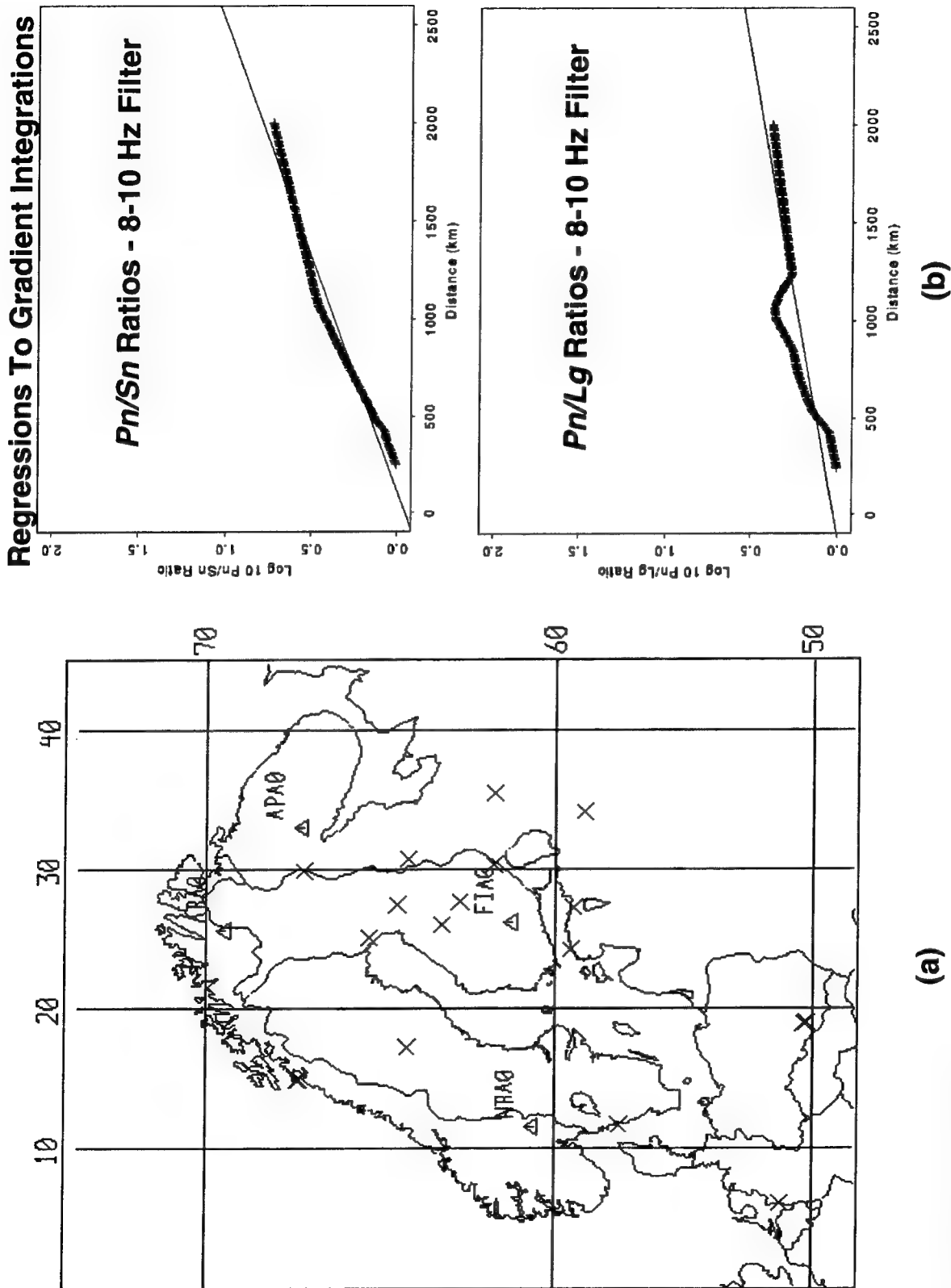
Figure 4:(a) Locations of events and arrays used to derive frequency dependent *Pn/Sn* and *Pn/Lg* correction. (b) Examples of the distance dependent gradient integration regressions in the 8-10 Hz frequency band for *Pn/Sn* and *Pn/Lg* measured for the events shown in (a).

$$Slope = \pi f \log e \left[\frac{1}{Q_s U_s} - \frac{1}{Q_p U_p} \right].$$ (13)

Figure 4 (b) shows examples of this integrated log amplitude ratio as a function of distance for *Pn/Sn* and *Pn/Lg* ratios measured in the 8-10 Hz frequency band. Each point in these plots represents the integrated gradient measurement over 10 km distance intervals. As shown, the points nearly line up on a linear trend, which we fit by least squares. This same linear trend was fit for the other 8 frequency bands.

Figures 5(a) and (b) show the family of curves which were derived from this analysis for *Pn/Sn* and *Pn/Lg* in the nine filter bands. All frequency bands have the same exponentially increasing trend with distance, as required by (12) and (13). The highest frequencies, filter passband above 7 Hz, seem to have the smallest distance dependence. The lowest frequency in the *Pn/Sn* ratio (1.5 Hz) has the grestest frequency dependence which may be suspect because this frequency band generally has the lowest SNR for *Pn*. In the case of the *Pn/Lg* ratios, the greatest frequency dependence shows up in the bands centered between 1.5 and 5 Hz.

Figures 6 (a) and (b) show the slopes of the linear log-ratios versus distance fits as a function of center frequency for *Pn/Sn* and *Pn/Lg* ratio, respectively. There is a rough trend of the slope decreasing with increasing frequency, although there is considerable scatter, particularly in the middle frequency bands. Some of this scatter may be due to inconsistencies in phase picking and sparsity of phase picks for some distances. It should be noted that only 15 events were used in this preliminary analysis.

Although our data fits produced somewhat variable trends, they all predict an exponential, or concave up, distance trend for all frequencies. These trends are significantly different than the trends from (5) and (6) based on the Sereno (1991) relations, which sometimes predicted concave down trends, most notably for the *Pn/Sn* ratios. We call this method the **Exponential Method** because it assumes that amplitude ratios increase exponentially with distance. Since our curves are based on fits to actual data in Scandinavia, an exponential distance trend best fits both *Pn/Sn* and *Pn/Lg* ratios in Scandinavia over distance distance range of 200 to 2000 km.

17
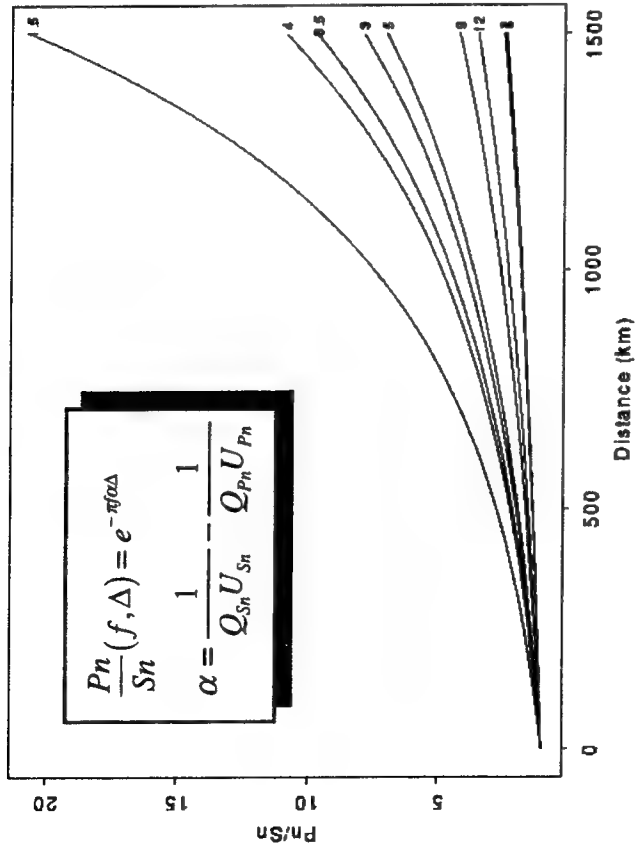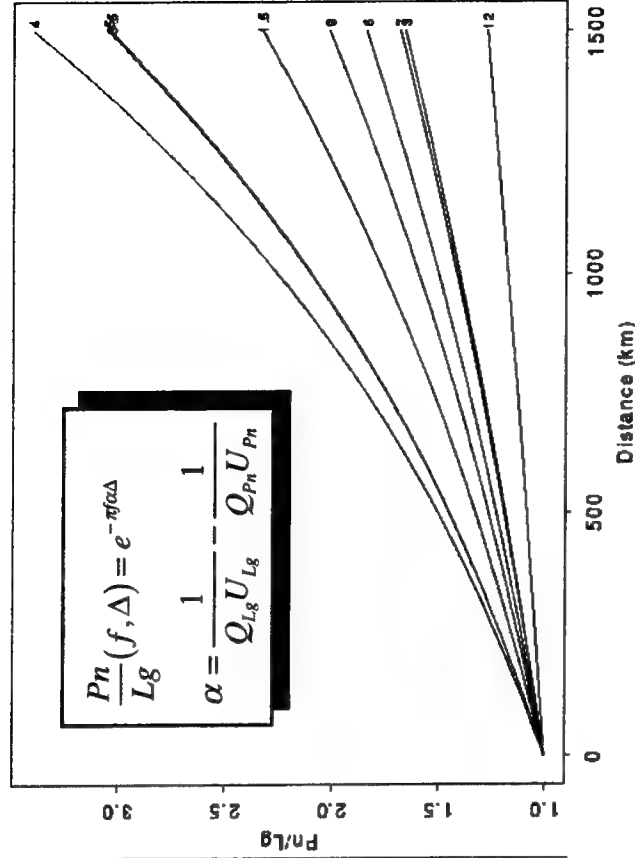
Figure 5: Frequency-dependent distance-correction curves derived for Scandinavia for maximum rms Pn/Sn (a) and Pn/Lg (b) amplitude ratios. Generally, the correction is larger for lower frequency bands.
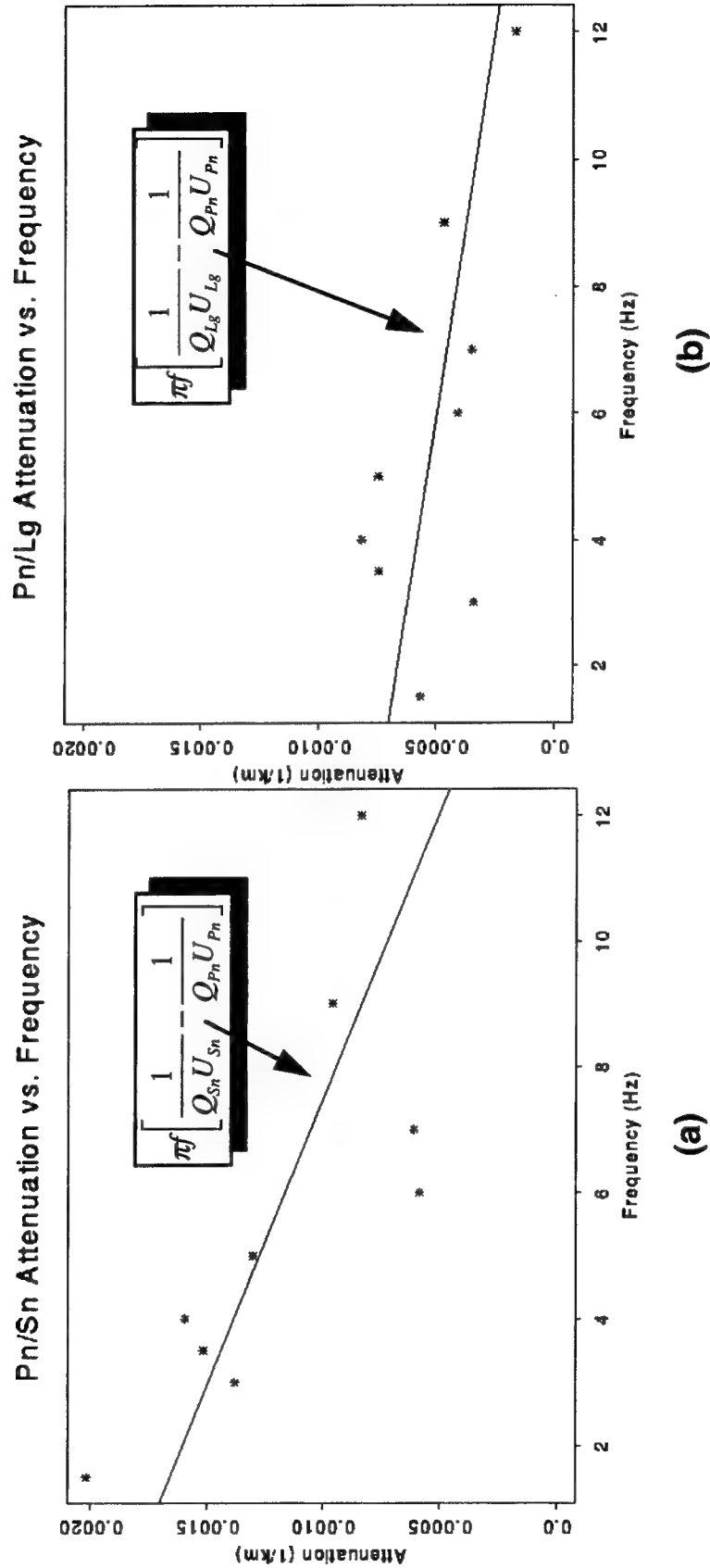
Figure 6: Exponential attenuation coefficients of the log max rms *Pn/Sn* (a) and *Pn/Lg* (b) amplitude ratios plotted versus frequency. Generally, the coefficients are larger for lower frequency bands, although there is considerable scatter. These coefficients apply to corrections at all distances in the Scandinavian shield.

19

3.3 Distance Dependence Correction Approach

We have implemented in ISEIS a distance-correction scheme for *P/S* amplitude ratios, using both approaches discussed above. Figure 7 shows the database indexing scheme we have developed for accessing and applying path corrections for amplitude-ratio features. The databasing scheme of ISEIS is based on the original CSS schema (Anderson et al, 1990) with extensions described by Baumgardt et al, (1991). The source parameters of seismic events which have been located by IMS are stored in the ***ORIGIN*** relation, indexed by a unique *Orid*. As shown in Figure 7, we assign events to reference regions, described by the ***REFREGION*** relation, indexed by a unique *Regid*. Reference events are defined by ***REFEVENT*** that has the *Orid* of the event and the name of the station, with abbreviation *Sta*. Thus, ***REFEVENT*** assigns a specific source-receiver path to the reference region. We add a relation, ***TECTYPE***, which gives a tectonic name to the path from the station to the reference region. The ***TECTYPE*** names shown are "Shield," "Hercynian," "Caledonian," and "Cordileran," indexed by *Tectid*. The *tectid* is assigned to unique feature correction relation, ***FEATCORR***, which defines a method for correcting the feature for distance. Currently, we only have one ***TECTYPE*** instance, "Shield" (for Scandinavia), and two methods for correcting *Pn/Sn* and *Pn/Lg* amplitude ratios for distance, i.e., the ***Sereno*** and ***Exponential*** method, described above. These methods are algorithms used to correct the amplitude ratios to a reference distance.

This indexing scheme allows us to have any number of feature-correction methods assigned to any number of tectonic types. Thus, in our case, we have the two methods discussed above assigned to the "Shield" tectonic type, which is Scandinavia. We believe many feature correction schemes may be generic for specific tectonic types; i.e., amplitude-ratio path correction schemes which apply to the Scandinavian shield will also apply to other shield regions as well. Future research using data from other regions of the world will test whether this is true. However, our scheme allows new methods to be added as they are developed when more data from other regions becomes available.

Figure 8 shows an example of the application of the ***Exponential*** distance correction scheme to mesurements of *Pn/Sn* amplitude ratios, measured in the 8 to 10 Hz band for events, for the seismic events near Novaya Zemlya studied by Baumgardt (1993) and Fisk et al (1993), in their analyses of the December 31, 1992 event. This event is plotted as an asterisk at a distance of about 1100 km from ARCESS on the *Pn/Sn (8-10 Hz)* versus distance plot in Figure 8. In Figure 8(a), the predicted ***Exponential*** curve is plotted on the points, which is the 9 Hz curve in Figure 5b. Note that on this plot, the December 31 event falls above the earthquake group and overlaps the explosion group at a smaller distance from ARCESS. Note that although the curve seems to
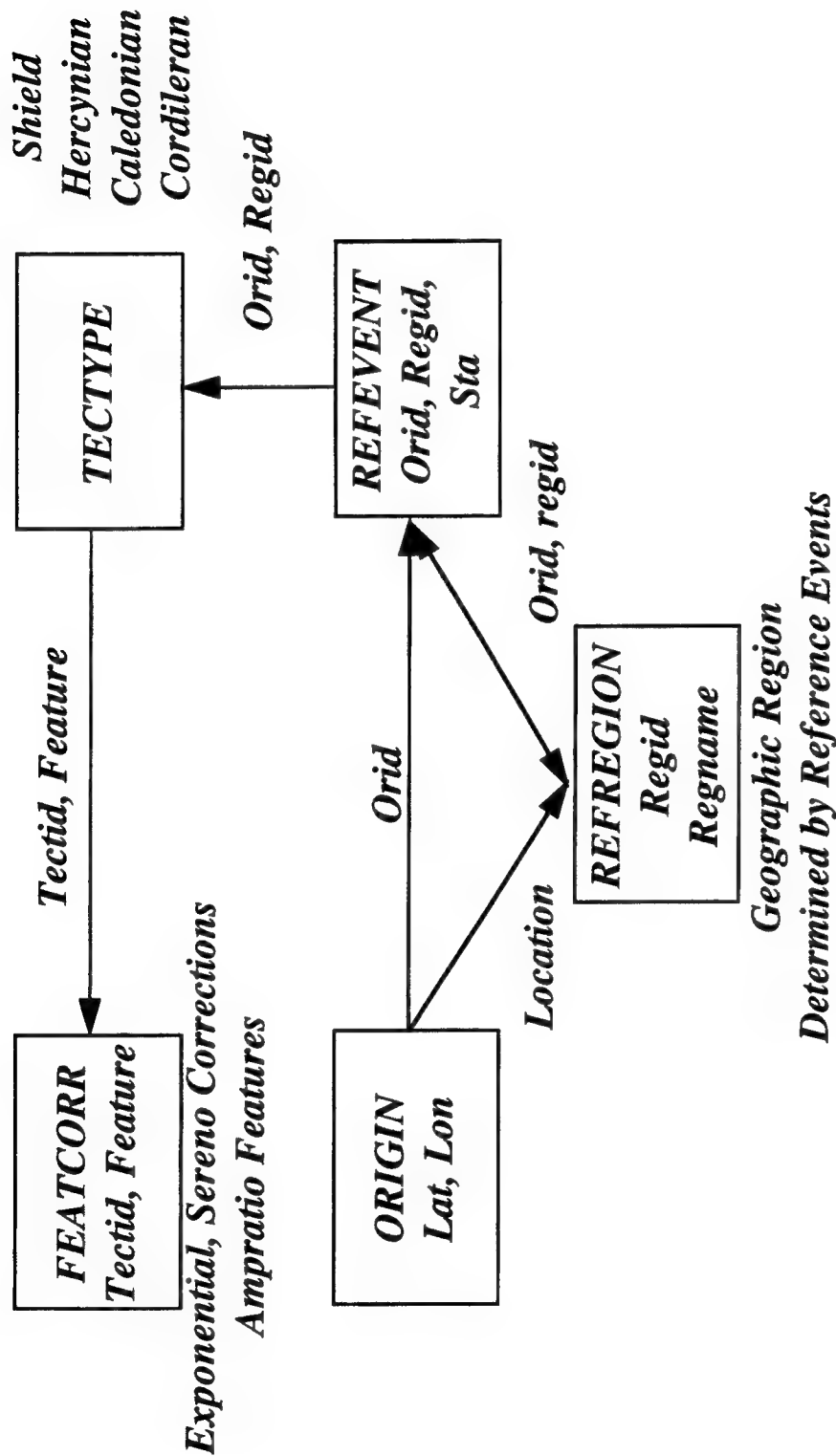
Figure 7: The *P/S* ratio correction indexing scheme for a station uses the Oracle database to store tables of reference events "indexed" to specific regions (*REFREGIONs*) which in turn point to tectonic types (*TECTYPEs*) that classify the tectonic region containing the refregion- to- receiver path. Tectonic types index relations that point to *P/S* corrections (*FEATCORRs*) which are methods for correcting the feature for distance. This indexing scheme allows us to study a number of different methods for making corrections.

21
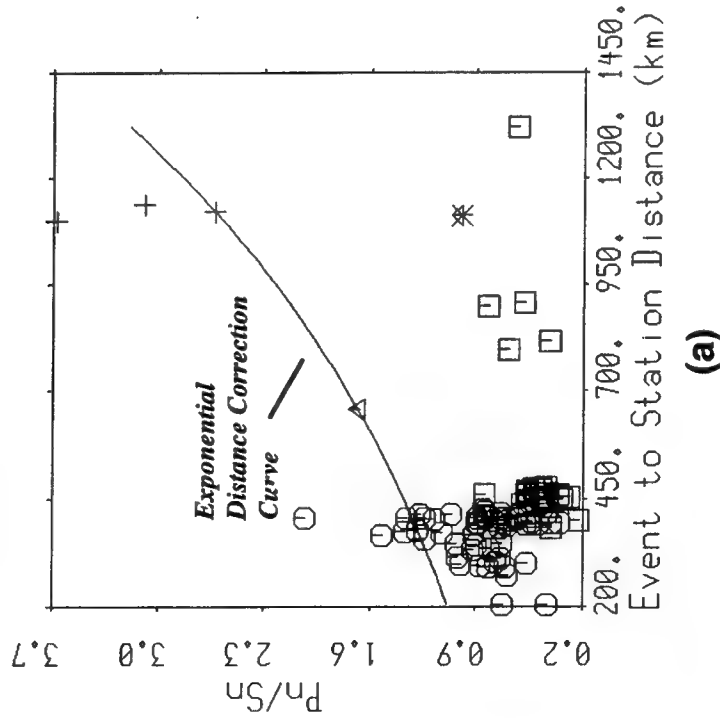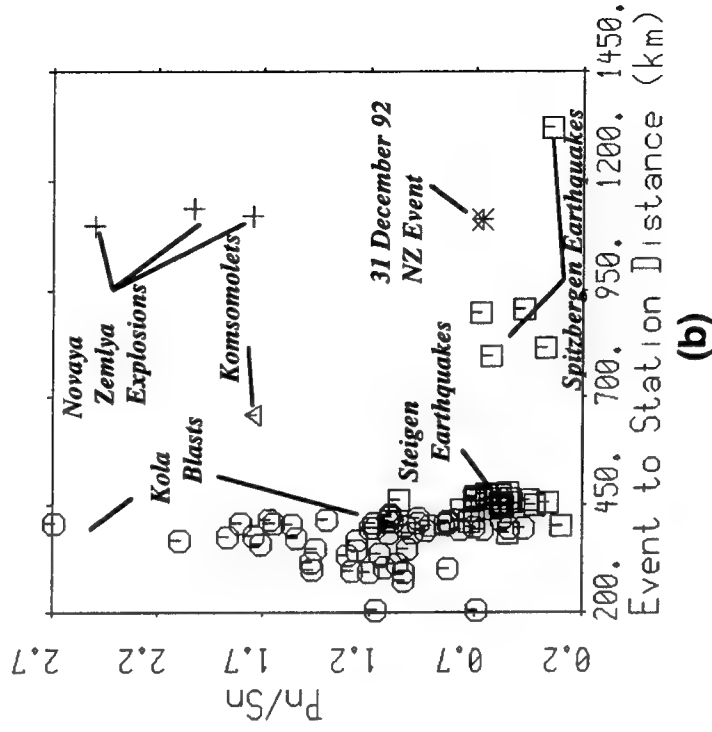
Figure 8: Examples of application of the exponential distance corrections for *Pn/Sn* ratios measured at ARCESS (From Baumgardt, 1993). (a) Plot of the distance correction curve for the 8-10 Hz band. (b) Same points as (a) but with the distance dependence of the curve removed. The correction moves the 31 December 1992 Novaya Zemlya event more into the earthquake group.

22

pass through many of the points, we are primarily interested in the shape of this curve for correction purposes, not its intercept with the vertical axis. Figure 8(b) shows the result of removing the exponential trend from the data points so as to shift the measurements to a standard distance of 700 km. When this trend is removed, we find that the December 31 point now shifts down and is more consistent with the *Pn/Sn* ratios of the earthquakes.

Figures 9(a) and (b) show the same analysis using the *Sereno* curve. Note in Figure 9(a) that the curve is concave down, as we discussed above, although the curve does seem to pass through many of the points. However, the trend in the *Sereno* curve over this distance range is not signifcantly different than our *Exponential* curve. Figure 9(b) shows the points corrected to the distance of 700 km using the *Sereno* curve. Again, the December 31 point is shifted down to be more in the earthquake category, as has also been shown by Fisk (1994). Although the shapes of the *Exponential* and *Sereno* correction curves are very different, the resultant corrections in this distance range have about the same effects.

The scatter in the data points in these plots is too large to make a case for either of the *Exponential* or the *Sereno* curves. This large scatter is caused by the separation of explosions and earthquakes provided by the high frequency *Pn/Sn* ratios. In fact, when the amplitude ratios are plotted on a log scale, which we normally do, both these curves are very similar since, in log space, they are linear with about the same slope. Thus, when extrapolating over short distances, either curve could be used for distance correction. In the next section, we show additional examples of these distance correction curves in log space for features extracted from other regions.

We emphasize that both of these sets of path correction curves should be regarded as preliminary and should only be used with care. Sereno's study (from which the *Sereno* correction curves were derived, was an assessment of regional detection capabilities of seismic networks for individual regional phases and did not directly address distance corrections for regional *P/S* amplitude ratios. Moreover, his study made assumptions about frequency-dependent magnitude source scaling. The *Exponential* approach does not require source-scaling assumptions. However, our *Exponential* curves are only based on analysis of 15 events, and more data needs to be analyzed to refine the curves. Also, we relied entirely on the IMS phase idenfications in generating these corrections. We plan later to verify the phase picks and redo the analysis, if necessary.

However, both these sets of curves represent a first step in developing path corrections for the amplitude ratios. Both these studies clearly show that amplitude ratios for *Pn/Sn* and *Pn/Lg* increase significantly with distances ranges over hundreds of km. Thus, when comparing

8.0 - 10.0 Hz

☐ : Earthquake
⊖ : Quarry Blast
△ : Marine Explosion
+ : Nuclear Explosion
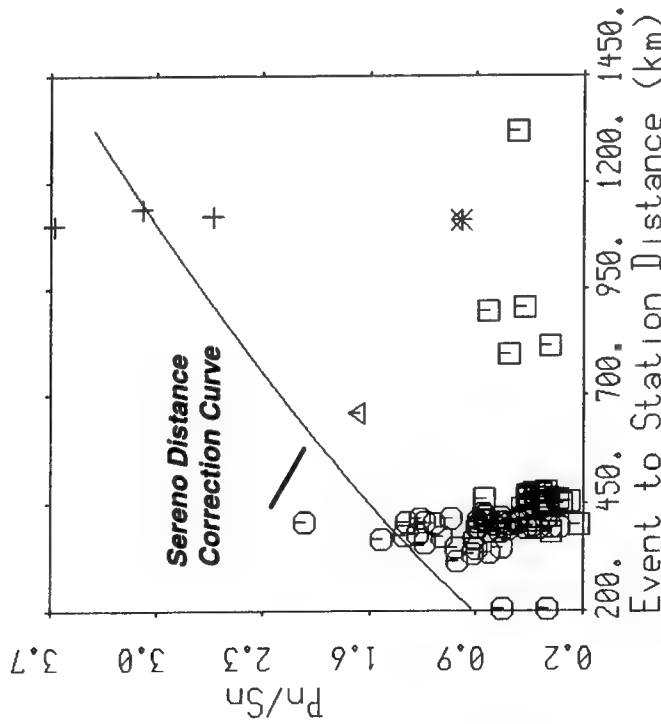
(a)

Pn/Sn

Sereno Distance
Correction Curve

Event to Station Distance (km)

200.   450.   700.   950.   1200.   1450.

0.2   0.9   1.6   2.3   3.0   3.7

8.0 - 10.0 Hz

☐ : Earthquake
⊖ : Quarry Blast
△ : Marine Explosion
+ : Nuclear Explosion
✛ : Unknown

(b)

Pn/Sn

Novaya
Zemlya
Explosions

Kola
Blasts

Komsomolets

Steigen
Earthquakes

31 December 92
NZ Event

Event to Station Distance (km)

200.   450.   700.   950.   1200.   1450.

0.3   0.9   1.4   2.0   2.5   3.1
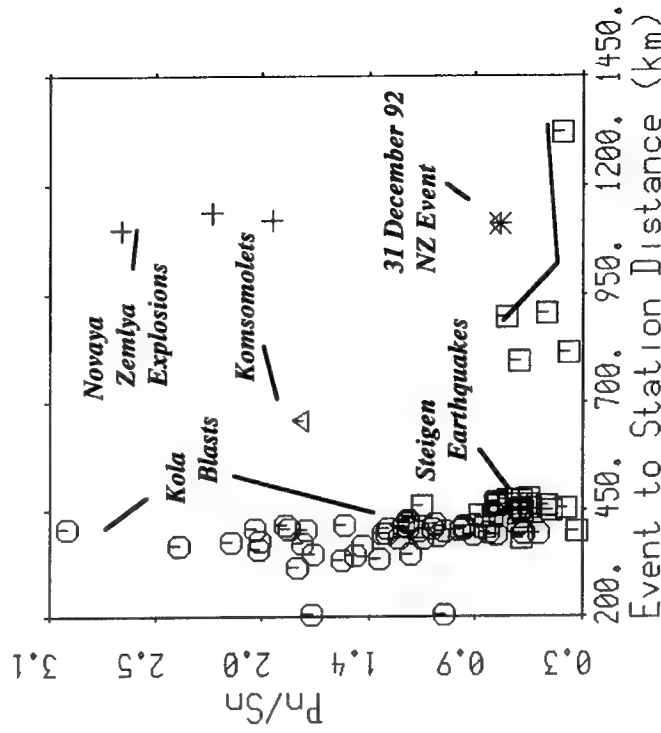
Figure 9: Same scatter plot as in Figure 8 but showing the *Pn/Sn* correction based on Sereno (1991). (a) Plot of the correction curve plotted on the scatter plot. Note that the curve trend is bending down rather than increasing exponentially. (b) After the ratios have been corrected to a distance of 700 km. As in Figure 8, after correction, the *Pn/Sn* ratio for the 31 December 1992 Novaya Zemlya event is closer to the earthquakes.

24

explosions and earthquakes which may be several hundreds of km apart, this differental attenuation of *Pn*, *Sn*, and *Lg* clearly needs to be corrected before the amplitude ratios can be used for discrimination.

4.0 TRANSPORTABILITY OF THE *Pn/Lg* DISCRIMINANT

In the previous section, we showed how to correct regional *P/S* amplitude ratios for distance, given that enough data could be analyzed to generate a reliable set of frequency-dependent distance trends for all the phase ratios of interest. However, we would expect that these curves might be quite different for different tectonic regions. For the Scandiavian shield, attenuation may be low for both *Sn* and *Lg*. However, for a more tectonically active region of the world, where there is active earthquake and volcanic activity, and hence, higher heat flows, we expect seismic attenuation in the crust to be higher. Thus, for a given distance and frequency band, we might expect *Pn/Lg* ratios to be larger in the tectonically active regions than for the shield at the same distance since, for the former, *Lg* would be more attenuated. Moreover, we would expect the distance dependence trend to be different for shield and tectonically active regions.

The other problem is the so-called "*Lg* blockages" which have been observed in continental areas, where tectonic boundaries of different kinds, such as sedimentary basins (Baumgardt, 1990), can either partially or completely eliminate the *Lg* energy. Blockages are difficult to correct by simple amplitude-distance curves because they may be very sudden and unpredictable. However, it may be possible to find where such blockages occur by examining crustal cross sections for the source-receiver propagation paths (Baumgardt, 1990). Once blockages are found the problem is how to calibrate *P/lg* ratio discriminants for blockages.

Thus, the problem of transporting discriminants between different geographic regions involves correcting the features for predictable effects due to differences in the tectonics of the different regions and the more unpredictable effects like blockages. It will not be possible to transport discriminants by just analyzing seismic data to calibrate a region, because in many regions, seismic data may be scarce. In this study, we have investigated using geological and geophysical data now becoming available from Geographic Information Systems (GIS), for regions of high interest, such as the Middle East, to correct for these effects.

4.1   Three Tectonic Regions

To investigate the transportability of the *Pn/Lg* ratio discriminant between different tectonic regions, we examine the variations of discriminants in three different tectonic regions, shown in the maps in Figures 10, 11, and 12. Each of the maps show the locations of events studied, and a number of the major tectonic features can be seen on the topographic color relief maps. These three regions have very different geologic and crustal structures.
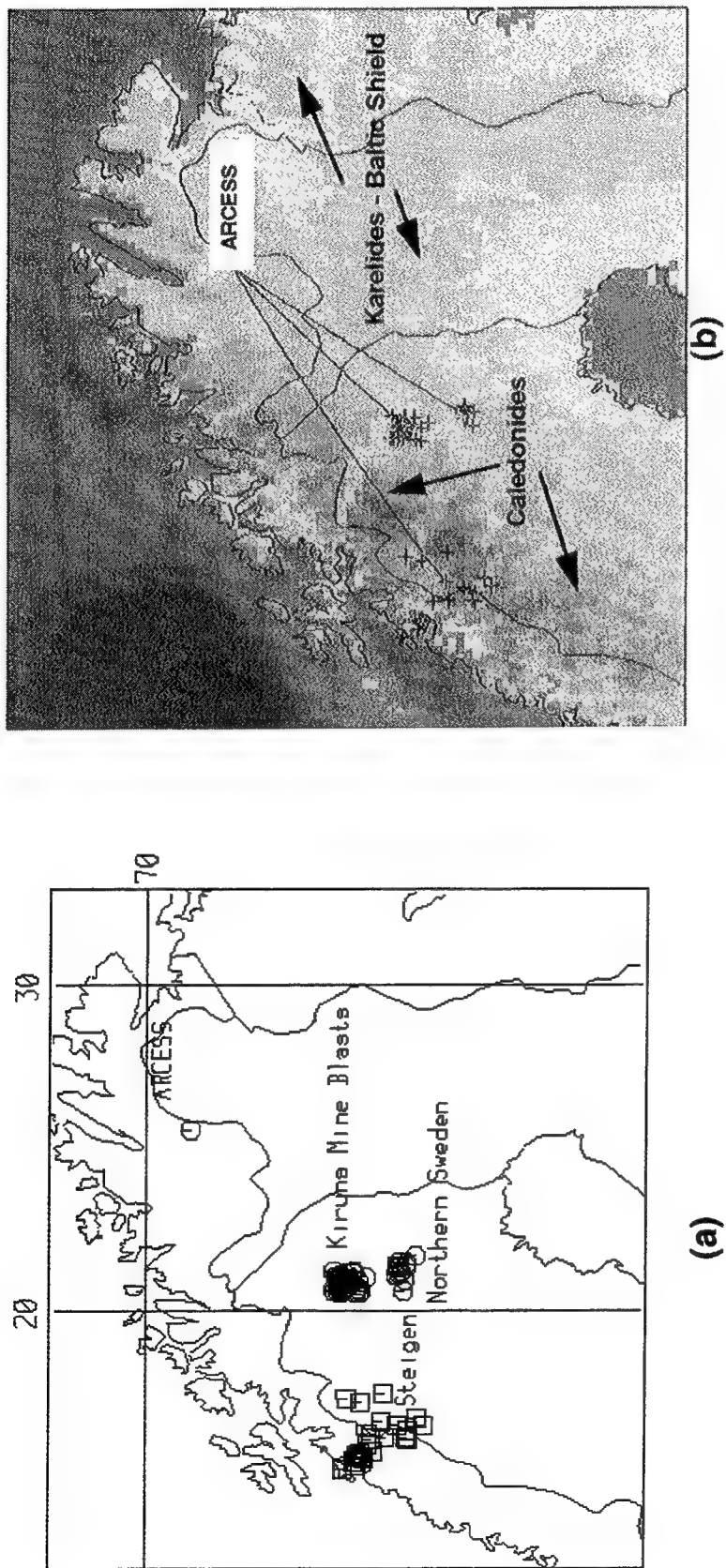
Figure 10(a) shows locations of mine blasts and earthquakes recorded at the ARCESS array in northern Scandinavia, where, as shown in Figure 10(b), the propagation paths cross primarily stable, shield-type tectonic regions, although the western part of Norway would be classified as a Caledonian Miogeosyncline (Kvale, 1976). These events have been analyzed by ISEIS in a number of studies (Baumgardt, 1993b).

Figures 11(a,b) show propagation paths to the GERESS array from mine blasts, earthquakes, and rockbursts in Germany, Poland, and Switzerland. The Vogtland events in Germany were originally studied by Wuster (1993) and in ISEIS by Baumgardt (1993b). The rock bursts and Swiss earthquake swarm events appeared in the Ground Truth Databases of Grant et al (1993) and the rockbursts were studied in ISEIS by Baumgardt (1993a). Figure 11(b) shows that these paths' cross regions characterized as shield and Hercynian orogens. The main tectonic feature in the region is the Tornquist Zone, which separates the Hercynian province from the western European platforms to the north (Watson, 1976). This region has been studied extensively by refraction profiles and shows a pronounced thickening of the crust (Guterch et al, 1986).

Figures 12(a,b) show propagation paths from earthquakes and nuclear explosions in China and Kazakh to the Chinese CDSN station, Urumchi (WMQ). The tectonic feature names on the topographic relief map are from Terman and Woo (1967). Most of the earthquakes come from the data lists of events previously studied by Bennett et al (1989). These include earthquakes in Tien Shan, Mongolia, and in the northern part of Tibet, and Russian nuclear explosions at the former Soviet test site in Kazakhstan (Balapan). We have added some additional more recent events, most notably, the September 29, 1988 nuclear explosion at Lop Nor, which had a magnitude of 4.7. To our knowledge, this is the only Lop Nor nuclear explosion for which seismic data has been made available from WMQ. These propagation paths cross tectonically active mobile belts. There have been many studies of the tectonics and earthquake mechanisms in this region of China (Tapponnier and Molnar, 1977; Molnar and Topponnier, 1978; Ni and York, 1978; Tapponnier and Molnar, 1979) which have shown that most of the earthquakes in these regions have normal and strike-slip mechanisms that are consistent with the convergence of Eurasia and India.

So, the crustal structures of the three regions shown in Figures 10, 11, and 12 progress from simple shield structures of Scandinavia (Figure 10), with little lateral heterogeneity in crustal structure, to more active tectonic structures with much more heterogeneous crustal structures of the region around GERESS (Figure 11) and WMQ in China (Figure 12). In this section, we compare the *Pn/Lg* ratio discriminant in these three regions and investigate to what extent the complex heter-

Tectonic Features and Propagation Paths

(b)

(a)

Figure 10: These maps show locations of the events at the Kiruna mine, the Steigen earthquake swarm and earthquakes and mine blasts in Northern Sweden. All events were recorded at the regional array, ARCESS. (a) Map showing region names and source types. Square symbols designate earthquakes and circles designate blasts. (b) Topographic map showing propagation paths from reference regions to the station. Most of the propagation paths cross stable platform or shield regions.

28

Tectonic Features and Propagation Paths
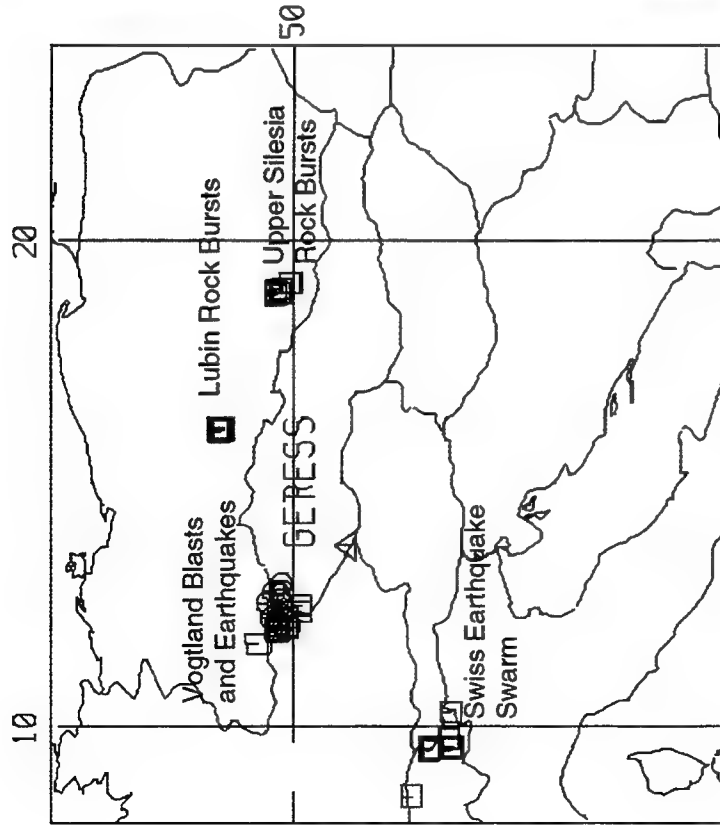
(a)
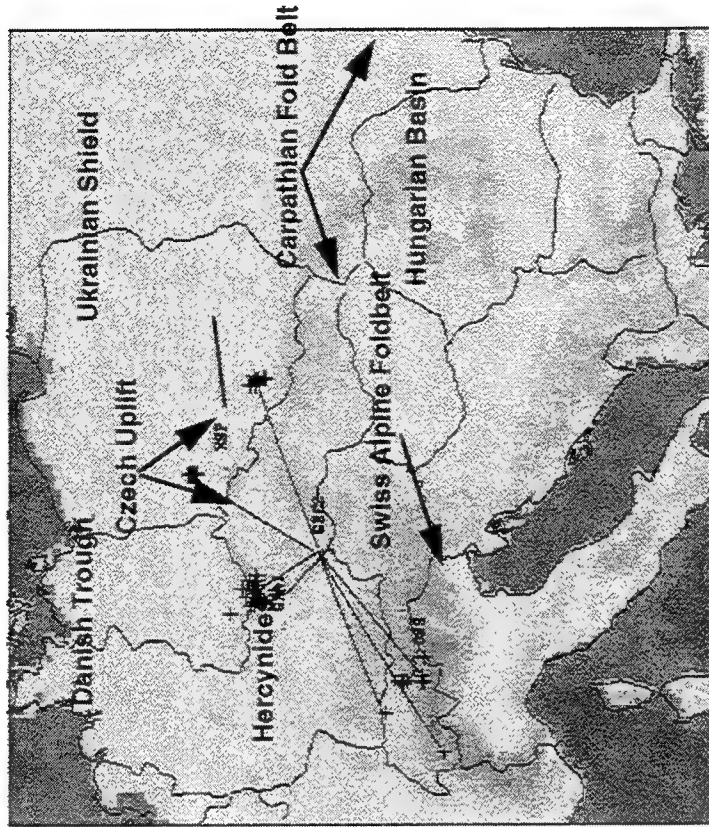
(b)

Figure 11: These maps show the locations of the Vogtland earthquakes and mine blasts, the Lubin rockbursts, the upper Silesia rock bursts, and the Swiss earthquake swarm. All events were recorded at the array GERESS. (a) Map showing region names and source types. Square symbols designate earthquakes and circles designate blasts. (b) Topographic map showing propagation paths from reference regions to the station. Propagation paths cross shield and tectonic crustal structures and sedimentary basins.

29

Tectonic Features and Propagation Paths

(b)

(a)
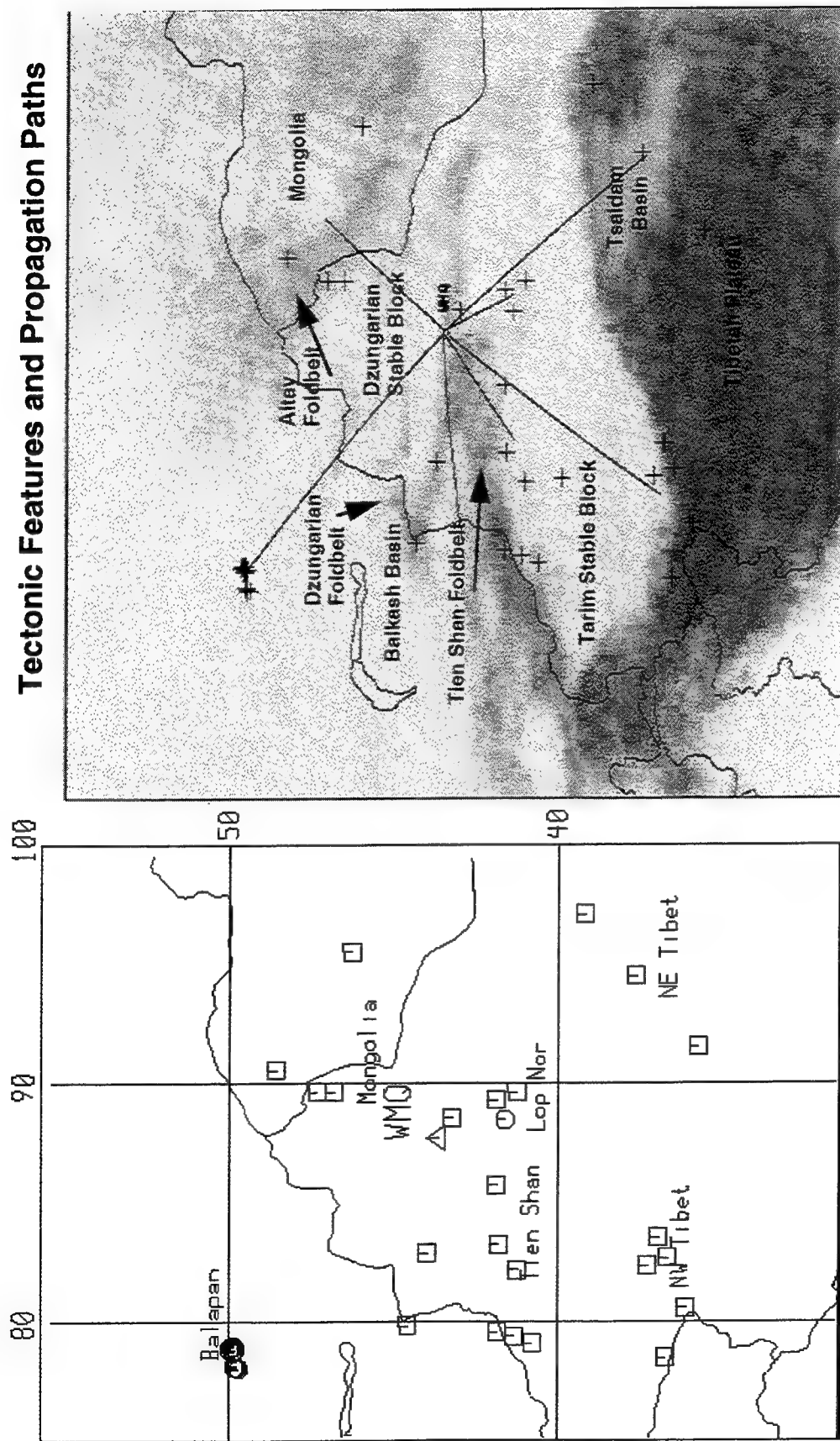
Figure 12: These maps show locations of earthquakes and nuclear explosions recorded at the CDSN station WMQ. (a) Map showing region names and source types. Square symbols designate earthquakes and circles designate blasts. (b) Topographic map showing propagation paths from reference regions to the station. Propagation paths cross a great diversity of tectonic boundaries, fold belts, and sedimentary basins.

ogeneous structures of the tectonically active regions affects the values of the *Pn/Lg* ratio and must be considered when transporting the discriminant from one tectonic region to another.

4.2 Basis for the *Pn/Lg* Amplitude Discriminant and Effects of Tectonic Structure

Figure 13 exemplifies the basis for the *P/S* ratio discriminant for identifying explosions and earthquakes. This figure compares an earthquake and explosion waveform in the Vogtland region of Germany recorded at one of the elements of the GERESS array. The two events are about the same distance (about 190 km) from GERESS and both events are in the same region which means that the seismic propagation paths to GERESS are about the same for the two events. On low frequency or broadband traces, both earthquakes and explosions produce sizeable *S* waves, although as shown in Figure 13, the amplitude of the *S* is far larger than the *P* for the earthquake as compared with the explosion, where the amplitudes are nearly the same. This is much more pronounced at high frequency (8-10 Hz) where the explosion *P* amplitude is nearly twice that of the *S* amplitude whereas for the earthquake, the *S* amplitude is still larger than the *P* amplitude. Also, the *P* wave is impulsive for the blast and emergent for the earthquake, an observation also made recently by Blandford (1993) who suggested it may be the basis of a regional complexity discriminant.

Figure 14 shows a similar comparison for the Lop Nor nuclear explosion in China and one of the nearby earthquakes in Tien Shan recorded at WMQ. These two events are about the same distance from WMQ that the blast and earthquake are from GERESS in Figure 13. The Tien Shan earthquake waveform in Figure 14 is very similar to the Vogtland earthquake waveform in Figure 13. In both cases, the *S* wave is larger than the *P* wave and the *P* onset is emergent. However, we note that the Lop Nor event has a much larger *P* wave than *S* wave, even at low frequency. The nuclear explosion in this case seems to be just a *P* wave source and generates a very weak *S* wave in all frequency bands. It would appear, then, that the nuclear explosion in China produces far less shear wave energy than a mine blast in Germany. Either nuclear explosions in general do not produce as strong shear waves as mine blasts or something in the propagation paths from Lop Nor to WMQ attenuates the shear waves from the Chinese nuclear explosion.

To compare nuclear explosions in two very different tectonic regions, Figure 15 shows a comparison of a nuclear explosion at Degelen, recorded at WMQ, and a Novaya Zemlya nuclear explosion, recorded at one of the elements of the ARCESS array. The two propagation paths cover about the same distance, 1000 km for Degelen to WMQ and 1100 km for Novaya Zemlya to

31
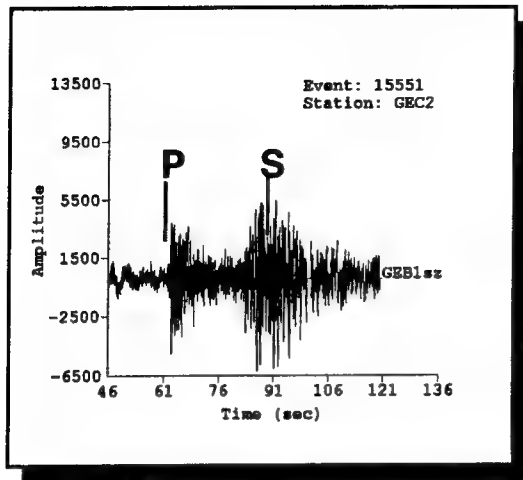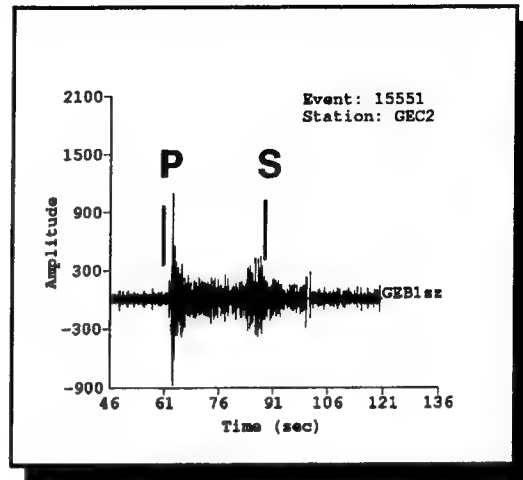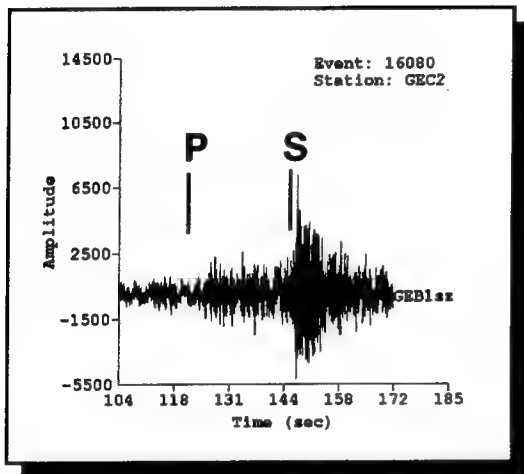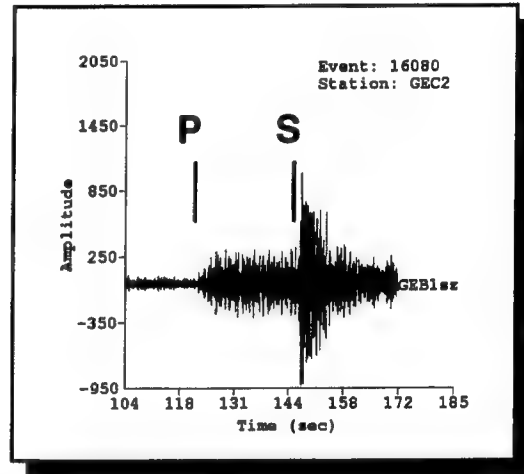
Figure 13: Examples of *sz* waveforms from a Vogtland mine blast and earthquake recorded at the GERESS array element GEC2. (a) Mine blast broadband seismogram (no filter), (b) earthquake broadband seismogram (no filter), (c) mine blast seismogram, 8-10 Hz filter, (d) earthquake seismogram, 8-10 Hz filter. At low frequency, both explosions and earthquakes generate strong *S* waves. At high frequency, explosions have much less *S* wave energy than earthquakes.
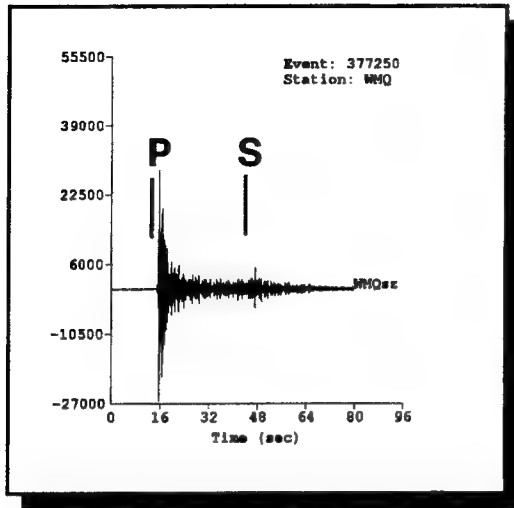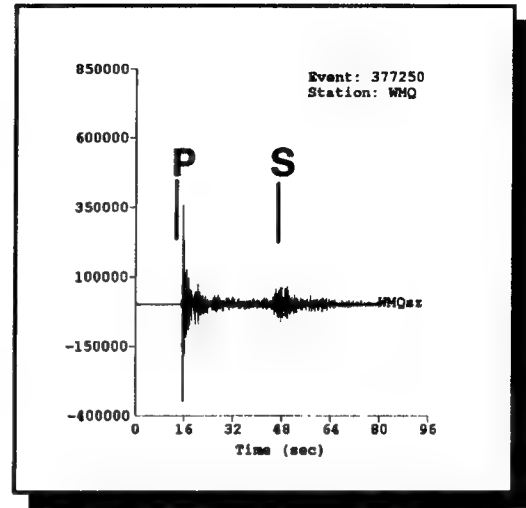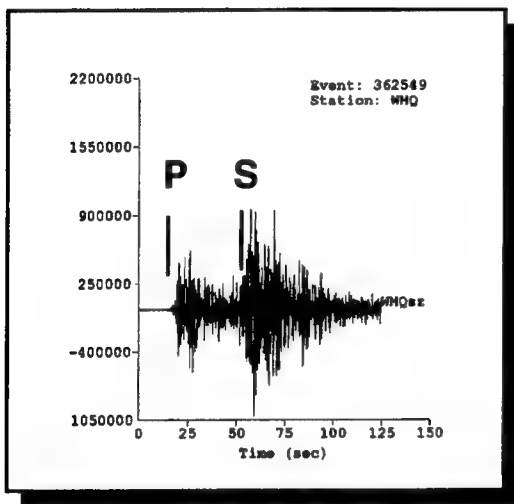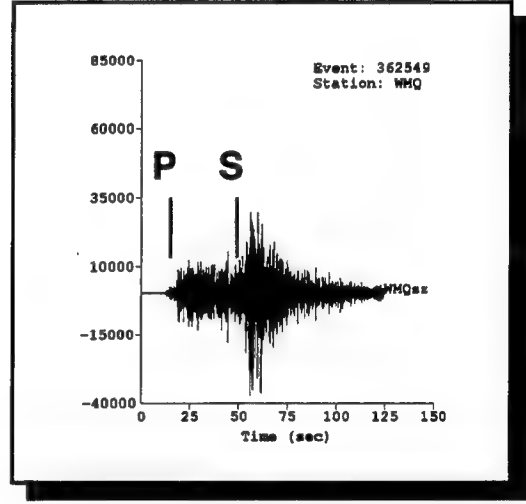
Figure 14: Examples of *sz* waveforms from Lop Nor nuclear explosion and a Tien Shan earthquake recorded at the CDSN station WMQ. (a) Nuclear explosion broadband seismogram (no filter), (b) earthquake broadband seismogram (no filter), (c) nuclear explosion seismogram, 8-10 Hz filter, (d) earthquake seismogram, 8-10 Hz filter. At both low and high frequency, the earthquake generates strong *S* waves but the nuclear explosion produces weak *S* waves.

ARCESS, but the crustal structures of the paths are very different. The propagation path cross sections for the two paths, obtained from the Cornell crustal structure database for Eurasia (Fielding et al, 1992), are also shown in Figure 15 and show the variations in topography, depth of sediments, and depth to the Moho along the two paths. Comparing the waveforms reveals that the Degelen nuclear explosion has strong *Lg* waves at low frequency, but no *Sn* wave is apparent. However, at high frequency, only a *P* wave is apparent. Evidently, the *Lg* wave is attenuated at high frequency and the *Sn* wave is unobserved at all frequencies in China. However, for the path from the Novaya Zemlya nuclear explosion to ARCESS, which is a shield path, there is no *Lg* wave observed but a strong *Sn* wave is observed at both low and high frequency. The propagation path cross section for the Novaya Zemlya-to-ARCESS path shows that there is a deep sedimentary basin in the path which apparently blocks the *Lg* wave at all frequencies. However, *Sn* propagates efficiently in all frequency bands.

These comparisons highlight the essence of the discriminant transportability problem. The regional phases *Sn* and *Lg* vary in their observability in different tectonic regions, and also their amplitudes will vary differently with distance and frequency, for reasons which are not always the same in all tectonic regions. The crust in China does not completely block *Lg* waves, although the anelastic attenuation of *Lg* in the crust seems to be high enough to eliminate *Lg* at frequencies above 5 Hz. However, mantle attenuation beneath China does not appear to permit *Sn* propagation over large distances. High-frequency *Sn* does propagate efficiently across the Barents Sea, perhaps because anelastic attenuation is low in the mantle beneath the region. However, *Lg* is completely blocked at all frequencies, not by anelastic attenuation, which is low in this region, but by being captured in the Barents Sea sedimentary basin, as discussed by Baumgardt (1990). Transporting the *Pn/Sn* or *Pn/Lg* ratio from one tectonic region to another requires careful accounting for these effects of the propagation-path structure on the amplitudes of the regional shear phases.

4.3   Analysis of the Lop Nor Nuclear Explosion - A Test Case for Discriminant Transportability

On September 29, 1988, a nuclear explosion test was conducted at the Chinese Lop Nor nuclear test site that had a body-wave magnitude of 4.7. The closest station to the Lop Nor test site is the CDSN station Urumchi (WMQ). Usually, this station is turned off by the Chinese during nuclear tests at Lop Nor. However, for this test, the station was left on accidentally. If the nuclear explosion had not been announced by the Chinese, the event might be considered a special event since it was recorded at WMQ which should only be on for earthquakes.

34

Seismograms

Crustal Cross Sections

Degelen → WMQ

**Degelen
WMQ Unfiltered
Strong *Lg*, No *Sn***

**Degelen
WMQ 8-10 Hz Filter
Lg Gone or Weak**

**Low Q Region
Sn Attenuated**

Novaya Zemlya

**Novaya Zemlya
ARCESS Unfiltered
Strong *Sn*, No *Lg***

**Novaya Zemlya
ARCESS 8-10 Hz Filter
Strong *Sn*, No *Lg***

**Barents Sedimentary
Basin - Lg Blocked**

**High Q Region
Sn Propagates**
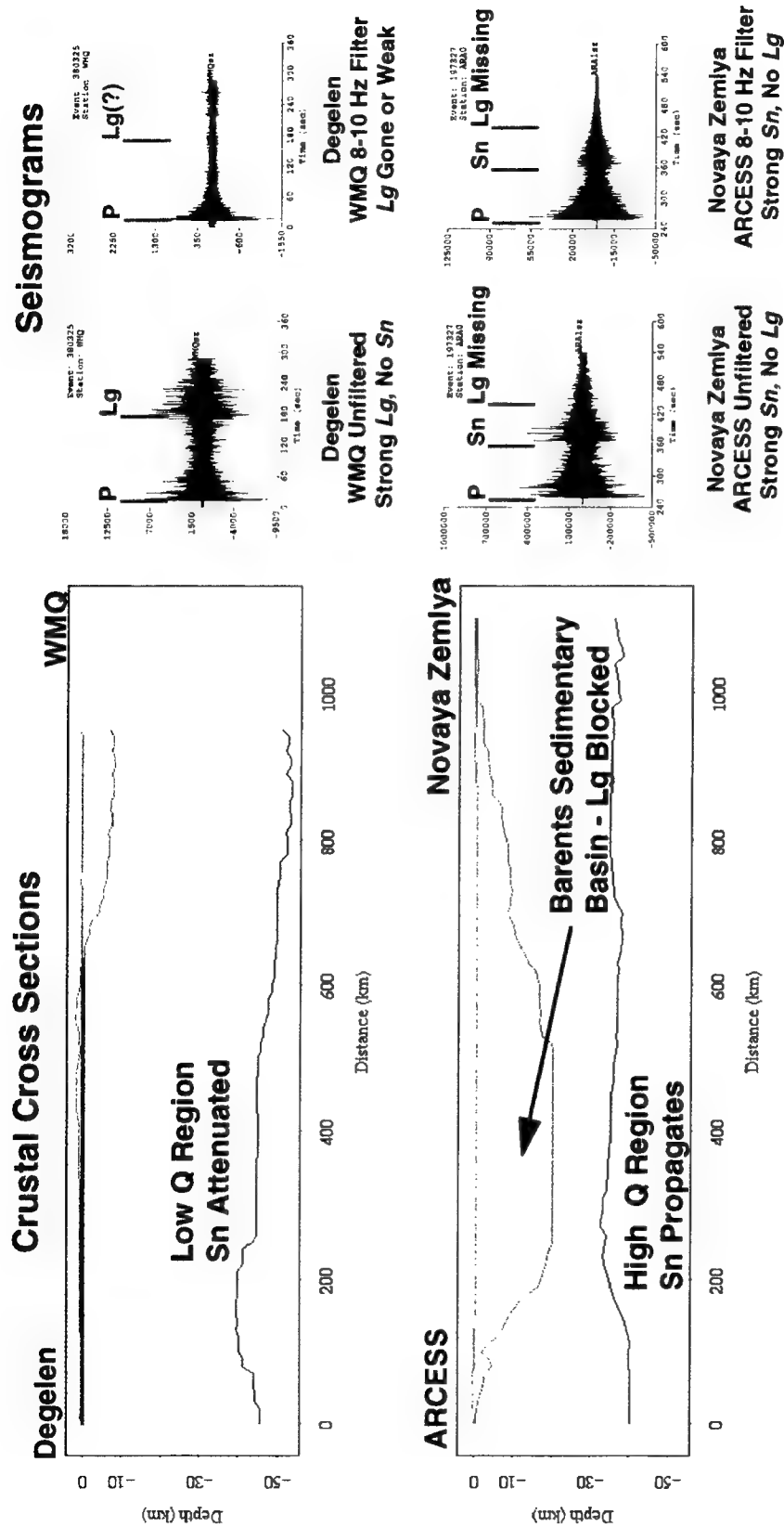
Figure 15: Comparison of propagation paths and waveforms for nuclear explosions at Kazakh recorded at WMQ and at Novaya Zemlya recorded at ARCESS. In China, *Lg* waves propagate at low frequency but *Sn* and high frequency *Lg* waves are attenuated. In Scandinavia, *Sn* waves propagate at all frequencies but *Lg* is blocked by the Barents sedimentary basin. These kinds of regional propagation effects need to be understood and considered when transporting the *P/S* discriminant from one region to another.

35

The characterization of this event relates to the transportability of regional discriminants because we have no other nuclear explosions at Lop Nor recorded at WMQ with which to compare the event. The distance of the event from WMQ is about 240 km. The maps in Figure 12 show that most of the events near Lop Nor are earthquakes. The Russian nuclear explosions at Kazakh are much more distant (about 1000 km) and the propagation paths from Kazakh to WMQ cross many complex crustal blocks. Thus, we can only compare the event to nearby earthquakes and much more distant nuclear explosions. To characterize this event, in order to identify it, assuming it had not been announced as a nuclear explosion, there would be two possible approaches:

(1)   Compare the *Pn/Lg* ratios of the event, recorded at WMQ, with nearby earthquakes recorded there and identify the event as earthquake if it is similar to the earthquakes. If not, the event might be characterized as anomalous or an explosion. To identify the event as a nuclear explosion, we must compare it with the more distant Russian nuclear explosions, which will require propagation-path distance corrections.

(2)   Compare the *Pn/Lg* ratios of the Lop Nor event with explosions and earthquakes recorded at comparable distance by some other station in some other part of the world. For example, there are earthquakes and mine blasts in the ARCESS and GERESS regions, as shown in Figures 10 and 11, which are in the same distance range as the Lop Nor nuclear explosion is from WMQ. Comparing the Lop Nor event recorded at WMQ with the events recorded at ARCESS and GERESS requires consideration of how the differences in the regional tectonics of the source and propagation paths will affect the discriminants.

This scenario may often happen in an actual CTBT or NPT monitoring situation, which might involve a "first test" in a country which previously has not admitted testing in a particular region. The test may be carried out in a seismically active region in hopes the test may be confused with an earthquake. The Lop Nor test site is located in eastern Tien Shan on the southern edge of the Dzungarian sedimentary basin in the vicinity of a number of seismically active faults (Tapponnier and Molnar, 1979). We first compare the Lop Nor event with earthquakes in this region as well as other more distant earthquakes in Tien Shan, Tibet, and Mongolia, and nuclear explosions in Kazakh. Then, we next compare the Lop Nor explosion with mine blasts and earthquakes recorded by GERESS and ARCESS at comparable distance but in different regions.

Comparison of the Lop Nor Explosion With Nearby Events

In this section, we discuss the ISEIS analysis of the WMQ recordings of the Lop Nor nuclear explosion and other events around WMQ, as recorded on both the short-period (40 Hz sampling rate) and broadband (20 Hz sampling) vertical-component channels at WMQ, referred to, respectively, as *sz* and *bz*. Wherever possible, we utilize data recorded on the 40 Hz *sz* channels, with Nyquist frequency of 20 Hz, which enables us to analyze ratios up to the 8-to-16 Hz band.

36

Figures 16 (a), (b), (c), and (d) show scatter plots of the *Pn/Lg* ratio, measured in the 8 to 10 Hz band as a function of region, magnitude, frequency, and epicentral distance, respectively. In each plot, the Lop Nor event is plotted as a star and is identified in Figure 16(a) as the CURRENT EVENT. Such plots are highly useful when characterizing special events in order to investigate all the factors which could be causing variations in the *Pn/Lg* ratios.

The first plot in Figure 16(a) compares the Lop Nor event with the other events on the basis of reference regions. The reference regions are identified as follows:

(1) *Lop_Nor* - This includes the Lop Nor event itself, indicated by the plus symbol, and four earthquakes, indicated by the squares. These earthquakes may be associated with left-lateral strike-slip faulting in the western Gobi desert (Tapponnier and Molnar, 1979).

(2) *Tien_Shan* - These earthquakes are located west of Lop Nor, in the Tien Shan fold and fault belt on the northwestern part of the Tarim Stable belt. Most earthquake mechanisms in this region are consistent with thrusting associated with the collision of the Indian plate with Eurasia (Ni, 1978).

(3) *NE_Tibet* - Three earthquakes located in the northeastern part of the Tibetan plateau, including one event in the Tsaidam sedimentary basin.

(4) *SW_Mongolia* - These earthquakes appear to be associated with the NW-SE trending right-lateral faults of the Altai foldbelt (Tapponnier and Molnar, 1979).

(5) *NW_Tibet* - These earthquakes are located in the northwestern part of Tibet, perhaps associated with the Altyn Tagh left-lateral strike-slip fault (Ni and York, 1978).

(6) *Balapan* - These are nuclear explosions of the former Soviet Union in the present-day Kazakh Republic. The "Balapan" region includes events at both the Degelen Mountain and Shagan River regions of the test site.

The region plot in Figure 16(a) shows the log10 *Pn/Lg* (8-10 Hz) ratios plotted as a function of these regions in order of increasing distance of the regions from the Lop Nor event. Figure 16(b) shows the same points plotted as a function of distance from WMQ. Since the Lop Nor event is also in the Lop Nor reference region, these two plots are very similar. The Scandinavian *Exponential* distance-correction curve for the 8-10 Hz *Pn/Lg* ratio, which was derived in the analysis described in Section 2.0, is overlayed on the points in Figure 16(b). This curve passes directly through the earthquakes in the distance range of about 400 to 1000 km, but it underpredicts the nuclear explosions and overpredicts the Lop Nor earthquakes. The two plots show that most of the earthquakes have log10 ratios between -0.5 to 0.4 over the distance range of 400 to 1000 km, with no strong systematic distance trend.

(a)

(b)
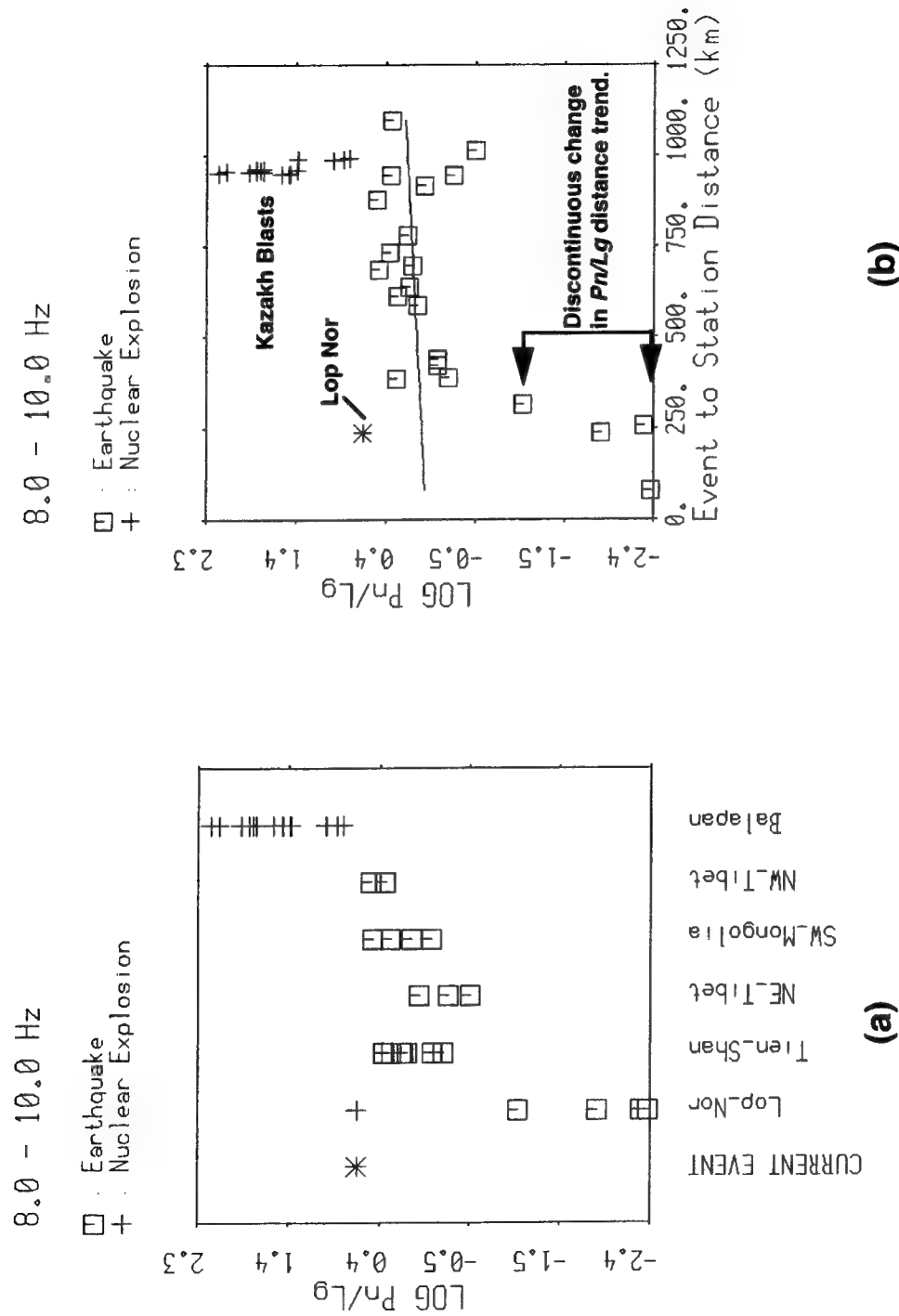
Figure 16: (a) Comparison of *Pn/Lg* ratios for Lop Nor Nuclear explosions recorded at WMQ with Chinese earthquakes and Soviet nuclear explosions. Regions are plotted in order of proximity to the Lop Nor event (CURRENT EVENT). Region plots may reveal regional variations in discriminant. This plot shows that Lop Nor earthquakes have unusually low *Pn/Lg* ratios. (b) *Pn/Lg* ratios plotted versus distance of the event from the station WMQ. The line is the Scandinavian distance correction for 8-10 Hz *Pn/Lg* ratios.
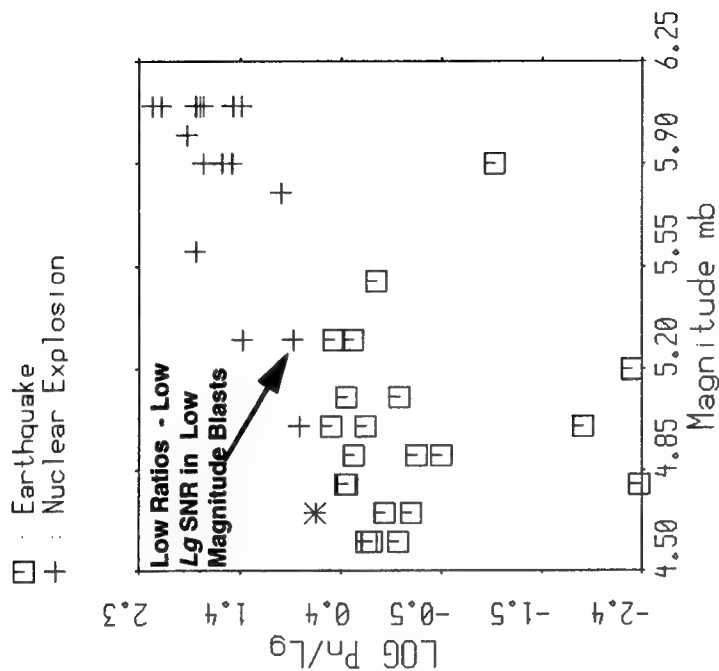
Figure 16: (c) Plot of Lop Nor *Pn/Lg* ratios vs frequency (star) compared with reference earthquakes (green) and nuclear explosions (red). Error bars show 2 sigma standard deviations. Frequency plots may indicate systematic frequency dependence of discrimination. Large *Pn/Lg* ratios in nuclear blasts indicate blasts are primarily *P* sources at frequencies above 6 Hz. (d) Plot of 8-10 Hz *Pn/Lg* ratios vs magnitude for Lop Nor blast (star) and reference earthquakes and nuclear explosions. Magnitude and SNR plots can reveal discriminant trends caused by magnitude variations.

39
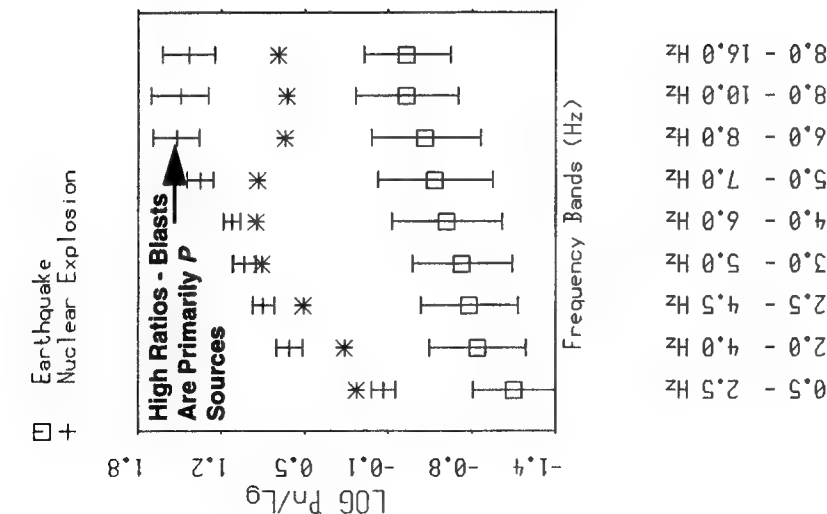
The striking anomalies in these plots are the very large *Pn/Lg* values of the Lop Nor and Kazakh nuclear explosions and the small values of the Lop Nor earthquakes. The waveforms for these events were shown in Figures 14 and 15. As pointed out earlier, nuclear explosions in Kazakh and China appear to be primarily *P* wave sources as recorded at WMQ. Thus, in the 8 - 10 Hz band, the large values of *Pn/Lg* ratio for both Lop Nor and Kazakh are due to the fact that *Lg* is very weak for the Lop Nor explosion and nonexistent for the Kazakh explosions. The small values for the Lop Nor earthquakes seem to be caused by strong *Lg* excitation at distances less than about 400 km. As shown in Figure 16(b), there appears to be a discontinuous change in the *Pn/Lg* ratio at distances beyond about 300 to 400 km. The strong *Lg* waves may be due to resonances and ground-motion amplification produced by sedimentary basins around WMQ. This point will be discussed again below.

Figure 16(c) shows the *Pn/Lg* ratio measurements, averaged over event type, as a function of the filter bandpass applied to the 40 Hz sampled *sz* data. Again, the star shows the measurements for the Lop Nor nuclear explosion. The error bars show two times the standard deviation of the measurements for all the earthquakes and nuclear explosions. The filter bands range from 0.5-2.5 Hz on the low end to 8-16 Hz on the high end near the 20 Hz Nyquist frequency. This plot shows roughly increasing ratios with increasing frequency. The greatest separation between the Lop Nor nuclear explosion and the earthquakes is apparent in the filter range centered about the 4 to 6 Hz band.

Figure 16(d) shows the scatter plots of the 8-10 Hz *Pn/Lg* ratios versus body-wave magnitude, *mb*. This plot suggests a possible systematic trend of increasing ratios with magnitude for the nuclear explosions but no systematic trend for the earthquakes. Also, Figure 16(c) shows that the ratios for the Lop Nor nuclear explosion decrease above the 6 to 8 Hz band, and the Kazakh explosions increase above this band. As we discussed above, nuclear explosions in Asia are primarily *P* sources at high-frequencies. In fact, above 8 Hz there is no *Lg* for the Kazakh explosions recorded at WMQ (see Figure 15). Thus, the ratios in Figure 16(d) for the nuclear explosions are actually *Pn/Noise* ratios, since there appears to be no *P* coda or *Lg* waves observed from the nuclear explosions above 8 Hz. Figure 14 shows that the Lop Nor nuclear explosion excites *Lg* waves, but they are very weak compared with the earthquakes. Therefore, Figure 15(d) shows that the apparent increase in the ratio is caused by the change in the *P* amplitude, relative to noise, in proportion to the magnitude of the event.

Finally, Figure 17 compares distance-dependent scatter plots of the 6-8 Hz log10 *Pn/Lg* ratio recorded in by the 20 Hz *bz* (a) with the 40 Hz channel (b) at WMQ. Superimposed on the
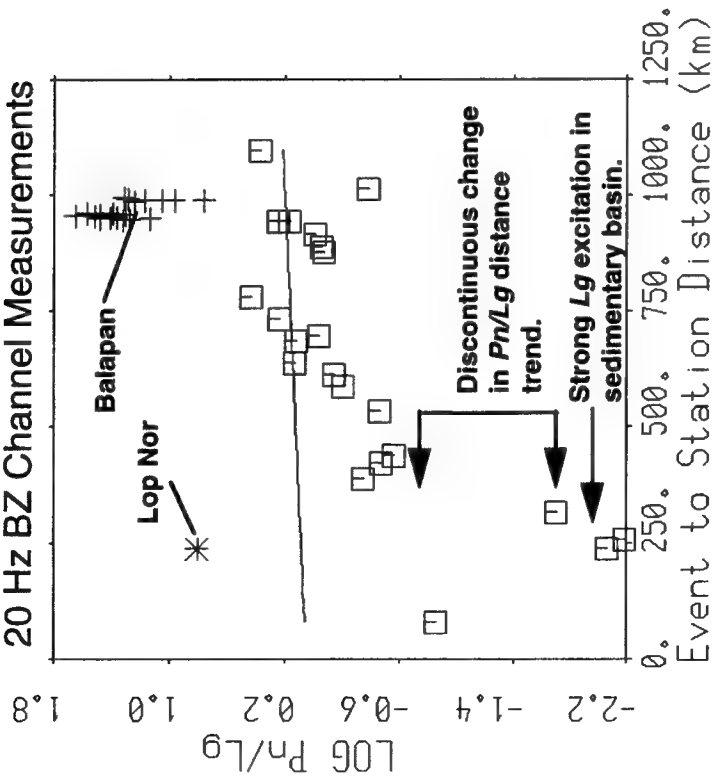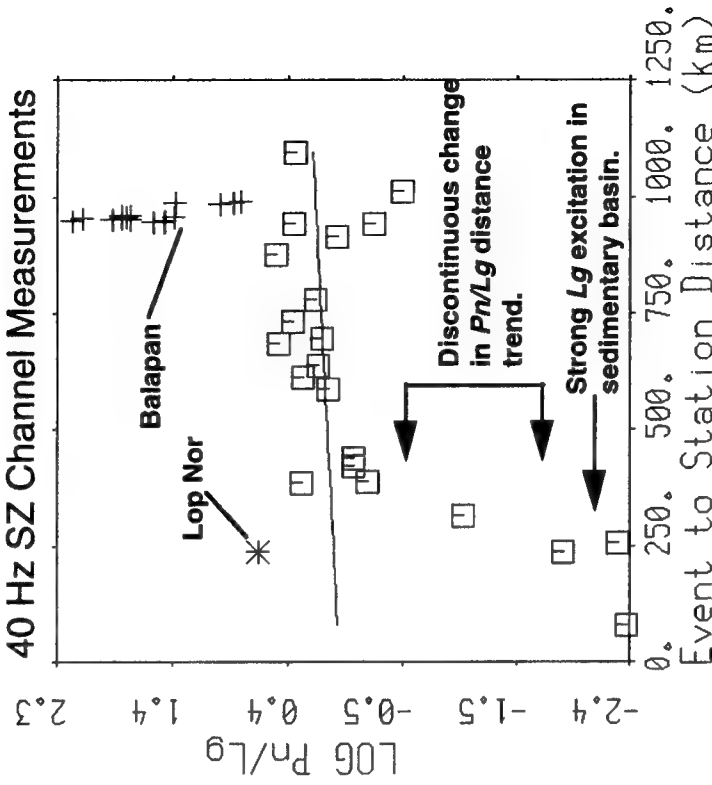
Figure 17: Comparison of plots of *Pn/Lg* ratio measured on the 20 Hz *bz* channel (a) and 40 Hz *sz* channel (b) at WMQ for earthquakes nuclear explosions in Eurasia. The astericks is the measurement for the Lop Nor nuclear explosion. Note the sudden jump in the ratios for the earthquakes at just beyond 250 km. Note that the Scandinavian distance correction curve almost fits the *sz* data for the earthquakes after the discontinuity.

41

plots are the Scandinavian distance correction curves for the 6-8 Hz band taken from the 7 Hz curve in Figure 5b. Both plots show very similar distance dependent trends at distances beyond 500 km. At closer distances, the 20 Hz data have somewhat smaller *Pn/Lg* ratios. However, both sets of measurements shows the clear anomalous change in the *Pn/Lg* ratio beyond 250 km.

Taken together, Figures 16 (a), (b), (c), and (d) and Figure 17 indicate clearly that the Lop Nor nuclear explosion would be identified as a pure compressional source. The earthquakes in the same region as the Lop Nor test site appear to be strong *Lg* sources, perhaps due to signal amplification in the sedimentary basins surrounding WMQ.

Comparison With Events in Other Regions

Figure 18 shows a comparison of the *Pn/Lg* (8-10 Hz) ratios for the Lop Nor event with measurements for events in the vicinity of GERESS (a) and ARCESS (b). The points in Figure 18 (a) come from a study which showed clear discrimination between earthquakes and explosions in the Vogtland region of Germany (Wuster, 1993; Baumgardt, 1993a) and comparison of two such events are shown in Figure 14. We also plot data points for rockbursts in Poland, first studied by Baumgardt (1993a) which show that these events look like earthquakes. The Lop Nor nuclear blast recorded at WMQ has a comparable distance to the Vogtland mine blast, and the value of the ratio is similar to the larger values of the Vogtland mine blasts.

Figure 18(b) shows the same comparison with the events in Scandinavia recorded at ARCESS, which includes blasts in the Kiruna mine of Sweden, other mine blasts and earthquakes in Sweden, and earthquakes in the Steigen region of Norway. Recently, these events were studied by Baumgardt (1994) who showed that the Kiruna blasts have large *Lg* waves, comparable to those generated by nearby earthquakes, which suggests that mine blasts can induce large shear waves, perhaps due to induced rock fracturing or spallation caused by ripple firing. These events have ratios which are well below those of the Lop Nor nuclear explosion, recorded at WMQ at comparable distance.

Thus, these two plots show that the *Pn/Lg* ratios for the Lop Nor nuclear explosion more closely resemble the GERESS recordings of mine blasts in Germany at comparable distance than the ARCESS measurements of earthquakes and blasts in Scandinavia. The lower values of the *Pn/Lg* ratio in the northern part of Scandinavia, as measured at ARCESS, may be due to the fact that the propagation paths have less *Lg* attenuation and blockage. As we showed in Figure 15, large *Sn* waves are observed at high frequency from nuclear explosions recorded in Scandinavia but not at WMQ. However, the Hercynian Province of Germany appears to be similar to the thrust

42
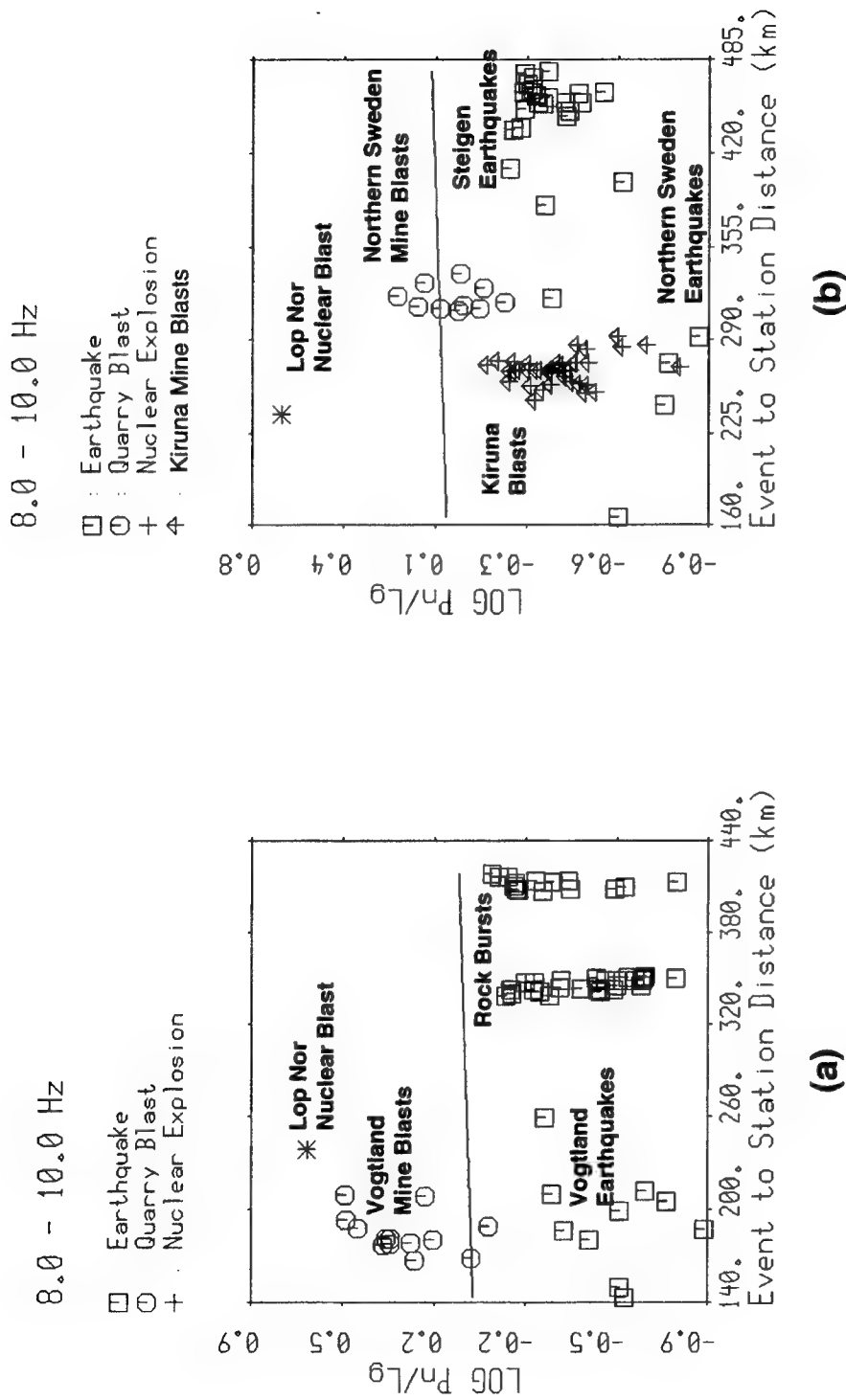
Figure 18: (a) Comparison of GERESS recordings of mine blasts, earthquakes, and rock bursts with WMQ recording of the Lop Nor nuclear blast. Mine blasts have lower *P/S* ratios which are closer to earthquakes and rock bursts. Perhaps mine blasts produce more shear waves as a result of ripple-fire induced cracking and spalling. (b) Comparison of ARCESS recordings of Scandinavian mine blasts and earthquakes with the WMQ recording of the Lop Nor nuclear blast. Scandinavian events have lower ratios perhaps due to more efficient *Lg* propagation in the shield. Note that Kuruna mine blasts (triangles) have *P/S* ratios comparable to earthquakes.

and fold belts of China in terms of the high attenuation of *Lg*. Thus, we would conclude from this comparison that discriminants are more transportable from the GERESS region to China than from Scandinavia to China.

4.4 Discriminant Transportability and Crustal Structure

Crustal Cross Sections

In this section, we investigate if knowledge of propagation-path crustal structure could be utilized to transport discriminants from one tectonic region to another. This idea was first considered by Baumgardt (1990) who showed that *Lg* blockage could be predicted by studying crustal cross sections of the propagation paths between the source and receiver, like those shown in Figure 15. The study revealed *Lg* blockage in the Barents Sea sedimentary basin between the Novaya Zemlya nuclear explosions and the NORESS and ARCESS arrays. More recent studies (Zhang and Lay, 1994 a,b; Zhang et al, 1994) have shown correlations between crustal structure features extracted from GIS databases (Fielding et al, 1992) and *P/Lg* ratio measured for stations over distances ranges of up to 2000 km. Strong correlations were observed between ratios in the 0.5 to 3.0 Hz band and variations in sediment thickness, topography, and measurements of *Lg* attenuation. However, because of the large distances involved, only low frequencies could be observed.

In this study, we apply the method of Zhang et al (1994) to ISEIS measurements of *Pn/Lg* ratios in frequency bands up to 10 Hz and look for correlations with crustal structure features. In order to ensure that both *Pn* and *Lg* waves are above the noise levels across this frequency band, we used only earthquakes in this analysis. The crustal structure features were derived from the Eurasian GIS database of Fielding et al (1992). Our intent in this study is to determine if there are measurable features in the propagation-path crustal structure which correlate with the *Pn/Lg* ratio features. If so, the *Pn/Lg* ratio feature may be "calibrated" to adjust the ratio when transporting it from one tectonic structure to another very different one. For the three structures in Figures 10, 11, and 12, we seek crustal parameters which correlate with the *Pn/Lg* ratio and can predict a "baseline" shift to adjust the *Pn/Lg* ratio for the Lop Nor event to allow it to be compared with explosions in recorded at GERESS in Germany or ARCESS in Scandinavia.

Another difference between our study and that of Zhang et al (1994) is that we only study earthquakes because we wish to look for correlations between crustal structure parameters and *Pn/Lg* ratios at frequencies up to 10 Hz. Because the nuclear explosions in China appear to have little or no *Lg* energy in this band, excluding the explosions ensures that there is sufficient signal-to-noise ratio in the *Lg* at high frequencies.

44

Figures 19, 20, and 21 show crustal cross sections from different "reference regions," defined by the seismic events in the regions, to the ARCESS, GERESS, and WMQ stations, respectively. These cross sections indicate the variations in topography, depth to sediments, if sediments are present, and depth to the Moho. The lines on the topographic maps between the stations and the specified regions are shown in Figures 10, 11, and 12. For this analysis, we categorize our events into geographic clusters using the ISEIS *reference region* concept, illustrated in Figure 7 and discussed in Section 3.3. The *reference regions* have centroid locations determined by the average location of clusters of events in the cluster and stored in the Oracle database in the *REFREGION* relation indexed by a unique *regid* number and a textual *regname*. Specific seismic events, stored in the database in the *ORIGIN* relation indexed by *orids*, are assigned to the *reference region* through the *REFEVENT* relation, which associates the *orid* and the *regid* and *sta.* (see Section 3.3 and Figure 7). In our analysis below, we examine the effects of propagation paths to *reference region* centroids on the average *Pn/Lg* ratio for the events in the region.

In Figure 19, the three propagation paths are from ARCESS to the average location of the Kiruna mine blasts reference region (*Kiruna*), earthquakes and explosions in northern Sweden reference region (*N_Sweden*), and the average location of the Steigen earthquake reference region (*Steigen*). Generally, these cross sections indicate that the crustal cross sections to all these reference regions have uniform thickness of about 40 km, with little topography and no sediments.

The reference regions in Figures 11 and 20 for GERESS are *Switzerland*, defined by an earthquake swarm in Switzerland, *Upper_Silesia*, defined by rockbursts in southeastern Poland, *Lubin*, defined by rockbursts in south-central Poland, and *Vogtland*, defined by the Vogtland earthquakes and blasts. These cross sections exhibit significantly more variation in crustal structure, as compared to the Scandinavian region around ARCESS, particularly in the crustal thickness. The crust is generally about 30 to 35 km for most of these paths to GERESS, except for the paths which cross the Swiss Alps, where the crust thickens to 50 km.

Finally, Figures 12 and 21 show the propagation paths and cross sections between WMQ and the reference regions in China, discussed above (*Lop_Nor*, *NW_Tibet*, *NE_Tibet*, *W_Tienshan*, and *Mongolia*). The former Soviet testsite, called *Balapan*, is also shown, although in this study, we exclude nuclear explosions). These regions show the greatest complexity in surface topography and sediment thickness, because the propagation paths in Figure 22 cross many foldbelts and sedimentary basins. Most notable are the sedimentary basins located

45
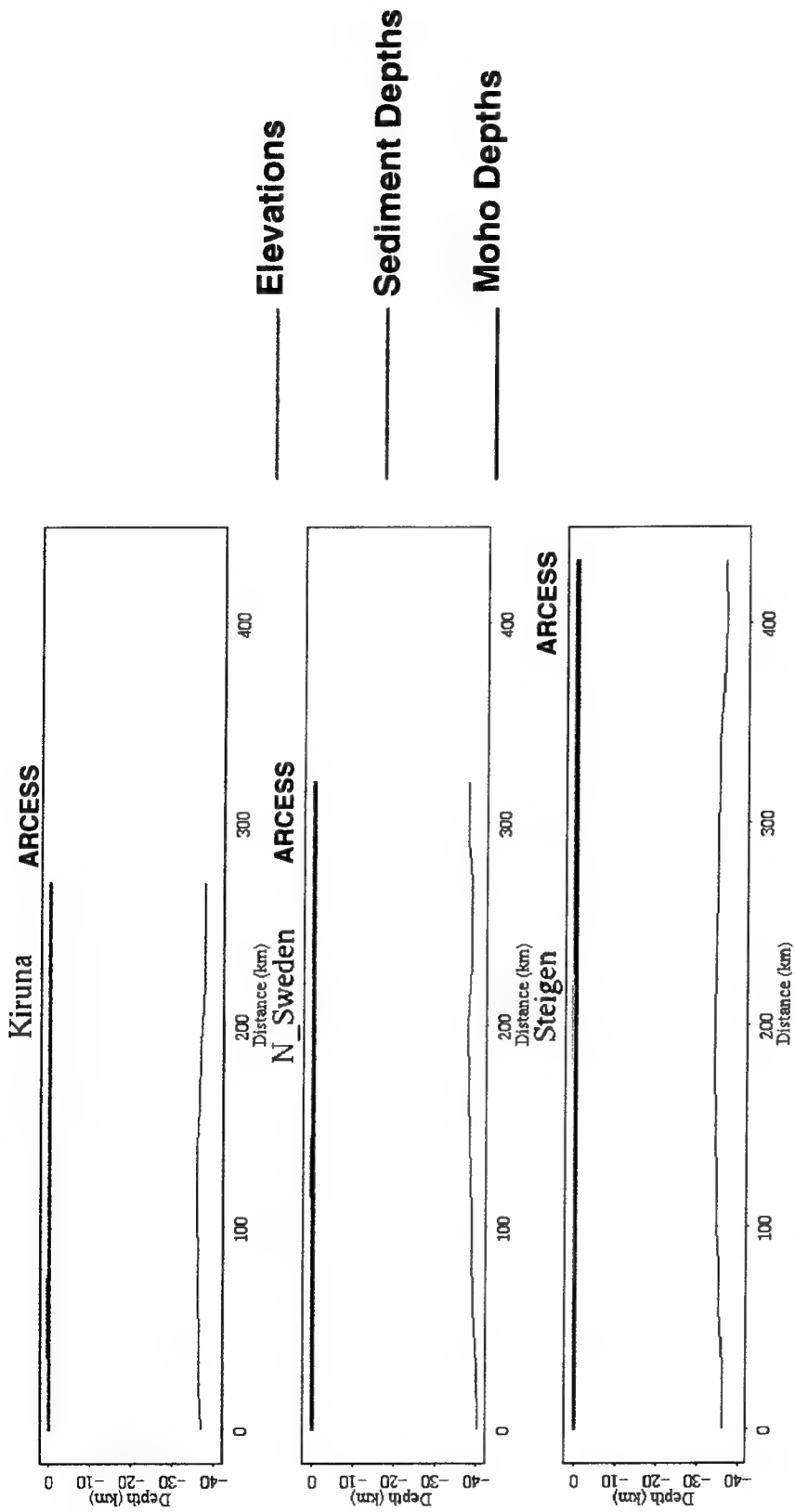
Figure 19: Propagation paths to ARCESS are nearly the same. They are very simple shield-type structures with no sediments or significant variations in topography. Crustal thickness averages at 38 to 40 km with minimal lateral variability.
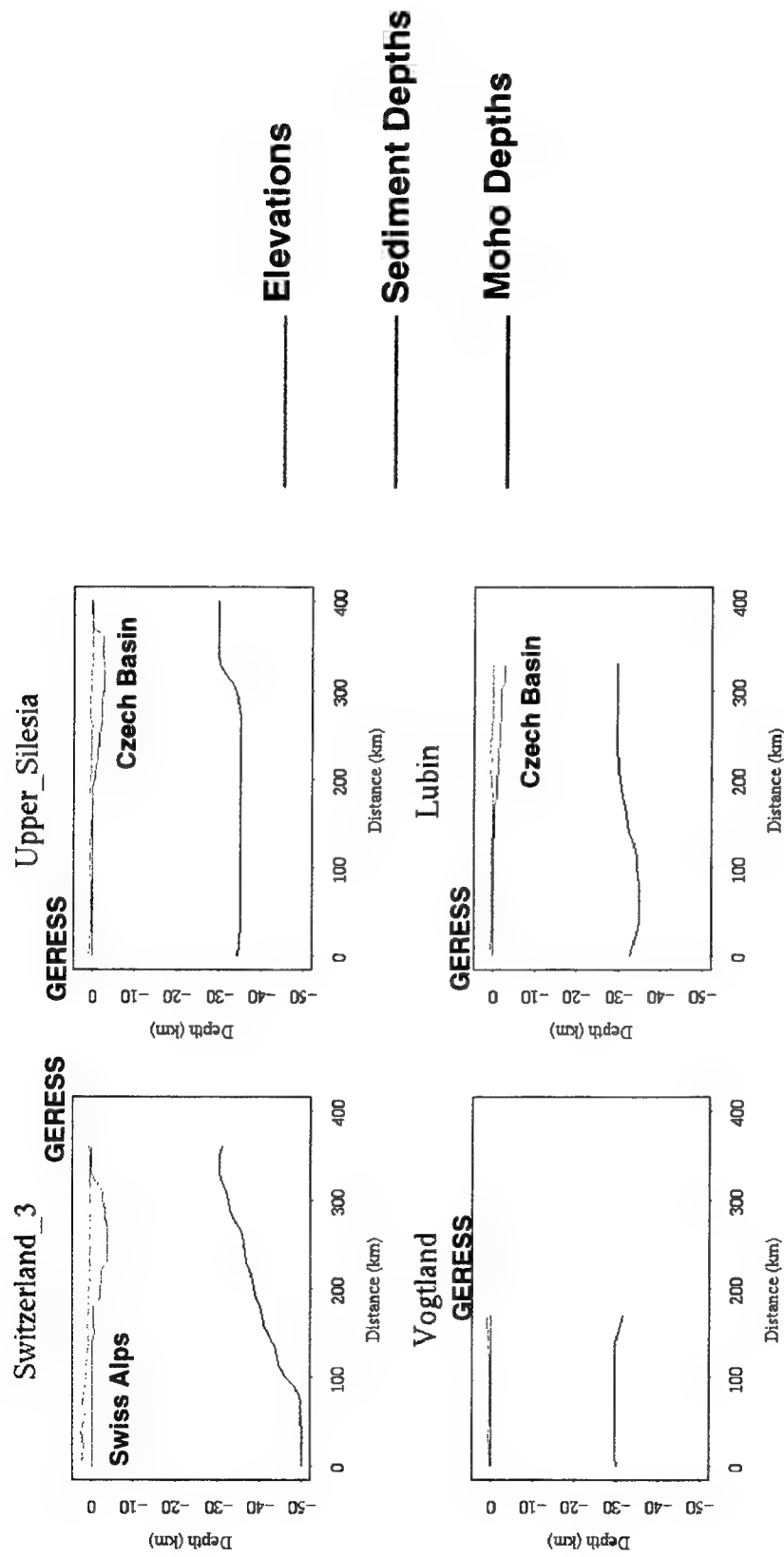
Figure 20: Propagation paths to GERESS display significant variability in crustal thickness, particularly for paths crossing the Alps. Vogtland paths are shield-like whereas paths from Upper Silesia and Lubin cross a small sedimentary basin, where sediments thickness reach 3 to 4 km.
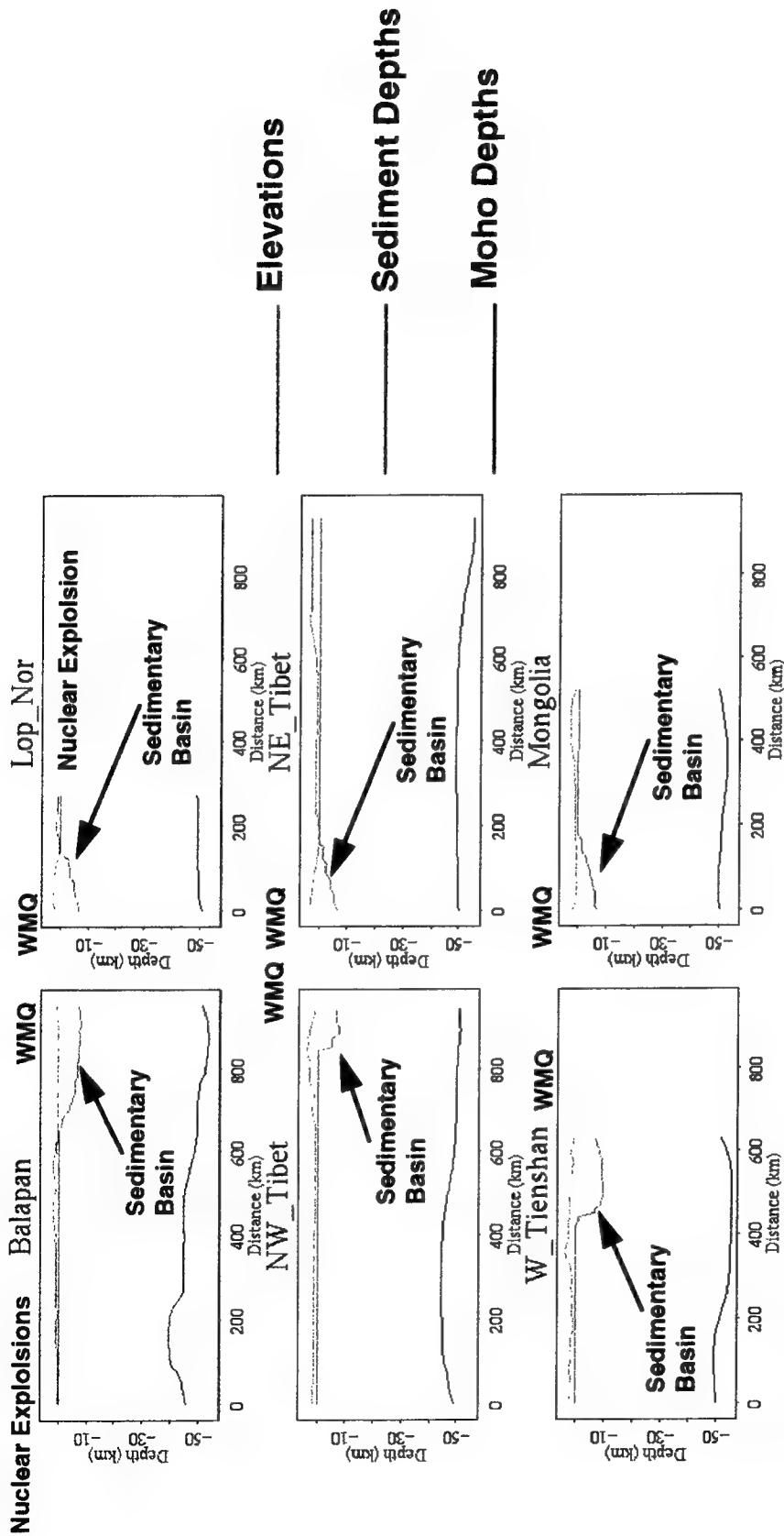
Figure 21: Propagation-path crustal cross sections for the Eurasian events (earthquakes and nuclear explosions) to the CDSN station WMQ. The position of WMQ on the cross section is shown. Note that WMQ and Lop Nor are located in the fault-bounded Dzungarian Stable Block basin where sediments reach 8 to 10 km thick. Events in the basin excite strong *Lg* waves which result in anomalously low *Pn/Lg* ratios.

around WMQ, which are the fault-bounded Dzungarian basin to the north and Tarim basin to the south.

It should be noted that the accuracy of these cross sections is variable. Although the Cornell group has tried to assure the reliability of the databases placed on their Internet server, the accuracy of the database is not always certain. For example, the digitized sediment thickness maps, from which the sediment thickness cross sections were derived, are gridded to 5' by 5' squares. For a particular cross section, this yields approximately 9 km accuracy in the distance position of the sediment thickness. We note in particular that the indication of thick sediments under WMQ is uncertain, since WMQ appears to lie on resistant sedimentary rocks in the foothills north of the Dzungarian basin (Francis Wu, personal communication). However, the Eurasian database indicates that it lies on up to 8 km of sediments above the crystalline basement, because of the low resolution of the sediment thickness database. Because the position of these sediments may be off by as much as 9 km, it would not be accurate to place WMQ inside a sedimentary basin itself, although it definitely lies within 8 or 9 km of the edge of the Dzungarian basin.

With the caveat that the present accuracy of the geological databases is limited, we present our approach to using crustal parameter correlations to calibrating the *Pn/Lg* ratio discriminant for different tectonic regions. The accuracy of the actual calibration in a region should improve as the accuracy of the GIS databases improve. At least this approach may provide a first order estimate of the calibration for regional tectonics.

Crustal Structure Parameters

Following Zhang et al (1994), we define the following crustal structure parameters derived from the propagation-path crustal cross sections:

(1) $E(\Delta_i)$ - The elevation, in meters, at the distance Δ_i from the station.

(2) $CT(\Delta_i)$ - The crustal thickness, in kilometers, at the distance Δ_i from the station

(3) $ST(\Delta_i)$ - The sediment thickness, in kilometers, at the distance Δ_i, from the station

These parameters are then averaged over each distance point along the cross section for the entire path.

Baumgardt (1990) suggested that it was the <u>change</u> in crustal parameter, in particular, changes in the sediment thickness above the basement, more than the mean value of the parameter

itself, which might cause blockage of Lg waves in continental areas. Zhang et al (1994) considered parameterizations of the maximum and minimum values of elevation and crustal thickness and maximum sediment thickness, in addition to the mean values. However, the maximum and minimum values may be redundant with the mean values. In this study, we investigate a different parameterization which is a more direct measure in the change in these features with distance, called the **average upper-quartile of the gradient**. To compute this parameter for each path, we first compute the gradient of the parameter at each distance point along the path as central difference derivatives, as follows:

(4) $\quad \nabla[E(\Delta_i)] = \dfrac{E(\Delta_{i+1}) - E(\Delta_{i-1})}{\Delta_{i+1} - \Delta_{i-1}}$ - The elevation gradient at distance point, Δ_i, in

units of meters/kilometers.

(5) $\quad \nabla[CT(\Delta_i)] = \dfrac{CT(\Delta_{i+1}) - CT(\Delta_{i-1})}{\Delta_{i+1} - \Delta_{i-1}}$ - The crustal thickness gradient at distance, Δ_i,

in units of kilometers/kilometer.

(6) $\quad \nabla[ST(\Delta_i)] = \dfrac{ST(\Delta_{i+1}) - ST(\Delta_{i-1})}{\Delta_{i+1} - \Delta_{i-1}}$ - The sediment thickness gradient at distance, Δ_i

in units of kilometers/kilometer.

For each distance point along the path, these central difference gradient values are computed. Rather than average these, we determine the upper quartile of these derivatives and average these values. Thus, the estimated gradient is an estimate of the largest gradients observed along the path. Averaging the upper quartile, rather than taking the maximum gradient, helps to avoid spuriously large values due to the limited resolution along the path.

Correlation Analysis

In the approach of Zhang et al (1994), crustal cross sections were determined for all paths between each source and receiver, and the parameters for each path were computed. As discussed above, we compute the crustal parameters for the propagation path to each *reference region* and examine the correlation between the mean values of the *Pn/Lg* ratio for the region and the crustal parameters for the path between the station and the reference region. Each of the parameters defined above are computed for each of the crustal cross sections shown in Figures 19, 20, and 21 and ISEIS used to measure and average the *Pn/Lg* ratios for the reference regions.

Figures 22, 23, and 24 show correlation plots of the average *Pn/Lg* ratio, measured in four frequency bands, 0.5-2.5 Hz, 2-4 Hz, 5-7 Hz, and 8-10 Hz, as a function of the mean values of

50
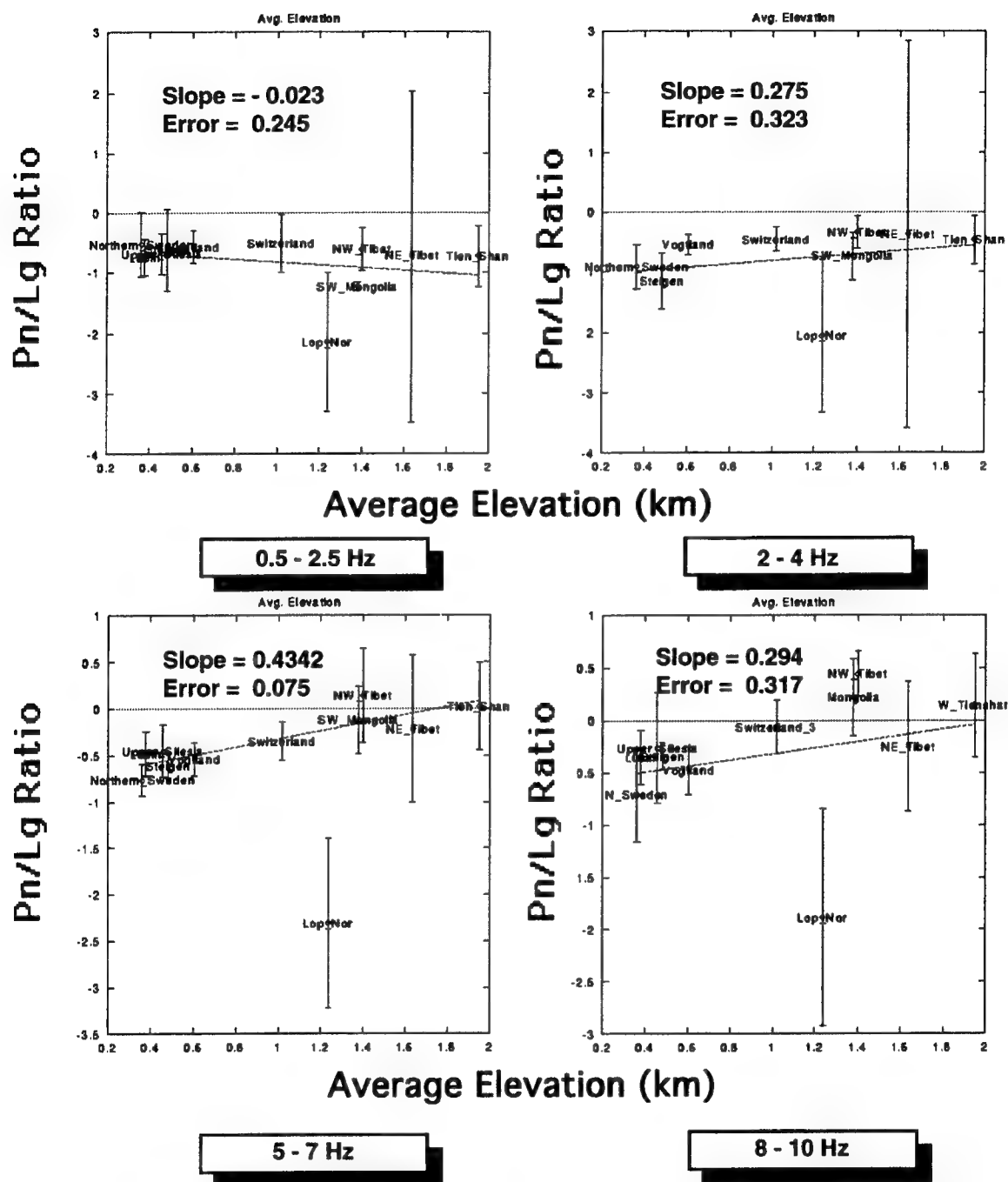
Figure 22: Correlation scatter plots of the log10 *Pn/Lg* amplitude ratios versus mean elevation along the propagation path.
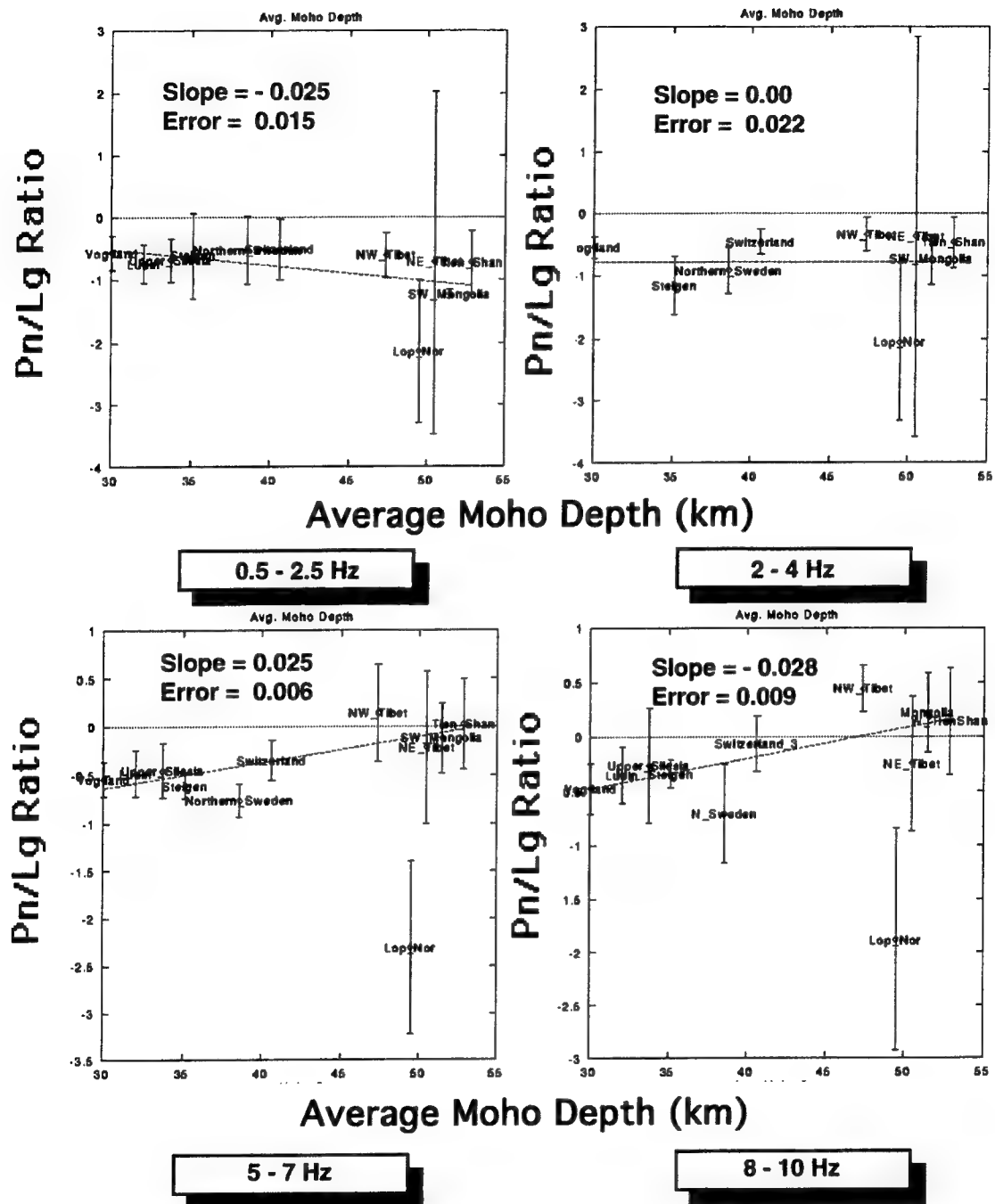
Figure 23: Correlation scatter plots of the log10 *Pn/Lg* amplitude ratios versus crustal thickness along the propagation path.
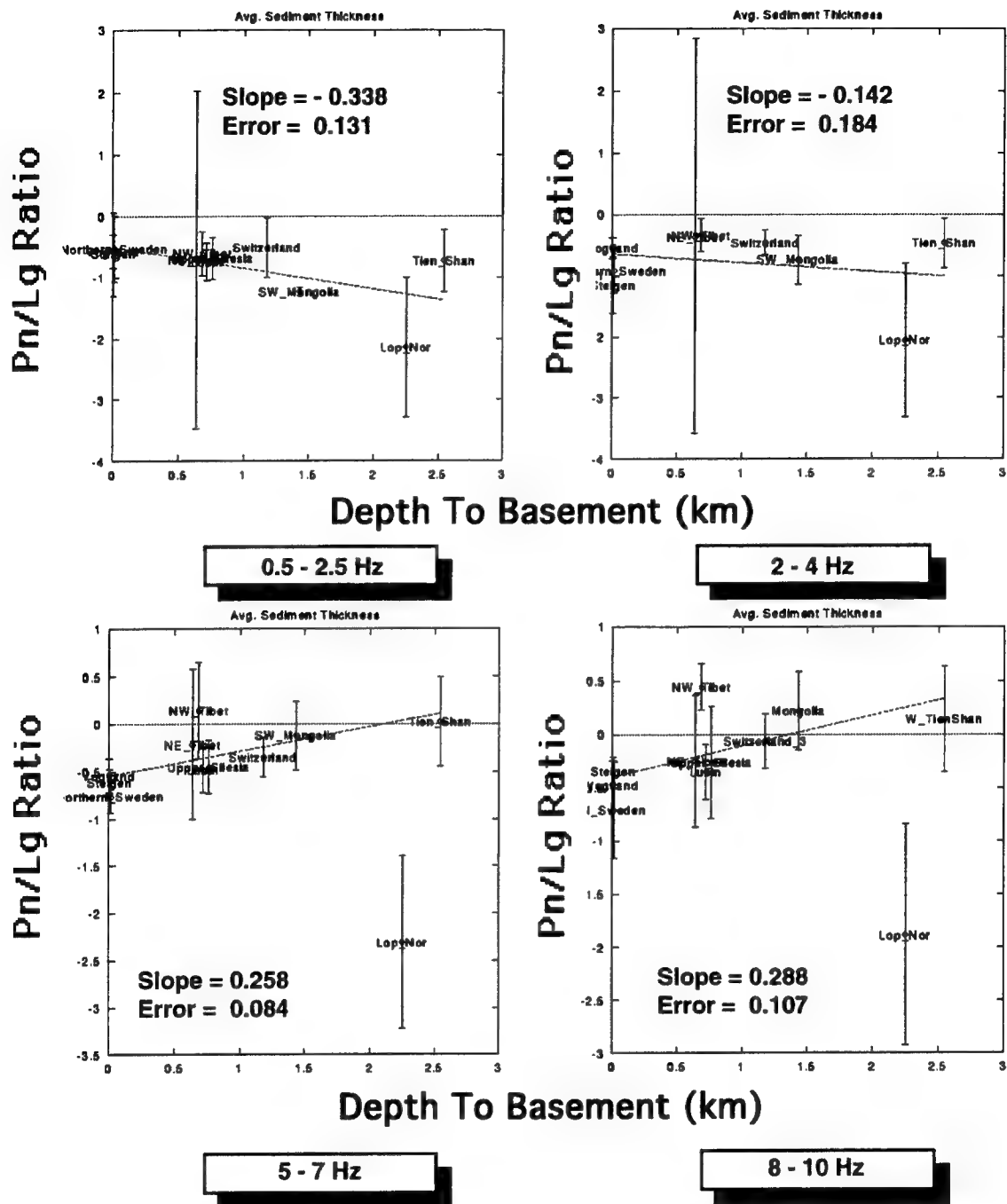
Figure 24: Correlation scatter plots of the log10 *Pn/Lg* amplitude ratios versus mean sediment thickness along the propagation path.

elevation, crustal thickness, and sediment thickness, respectively. Plots of the average of the upper quartile of the gradients of these parameters in the same four frequency bands are plotted in Figures 25, 26, and 27. The error bars on each point are the standard deviations about the means of the *Pn/Lg* ratio measurements for each reference region. For each plot, a straight line, determined by linear regression, is plotted through the points and the slope and standard errors of the regressions are shown on each plot.

In all these analyses, we find the best correlations with the high-frequency ratios (5-7 Hz and 8-10 Hz) both in terms of size of the slope and minimum error. The smallest standard-deviation error bars are found for the highest frequencies, with the exception of the Lop Nor region, where there are large variations in the *Pn/Lg* ratio, as we have discussed above. We discuss this error bar in more detail below. Most of the error bars indicate a scatter of on the order of +- 0.5 log *Pn/Lg* ratio units, which is comparable to the scatter found in the Zhang et al (1994) study.

At high frequency, the best correlated parameters are mean elevation, mean sediment thickness, and their upper quartile gradients of the parameters. The crustal thickness parameter shows very little, if any, correlation with *Pn/Lg* ratios. Baumgardt (1990) argued that *Lg* attenuation and blockage is primarily dominated by upper crustal effects, like the upper-crustal velocity variations caused by sedimentary basins and elevation changes. Depth to the Moho appears to have very little effect on the variations in *Pn/Lg* ratios.

To compare with the Zhang et al (1994) study, the 0.5 to 2.5 Hz *Pn/Lg* ratios are closest to the 0.5 to 3.0 Hz *P/Lg* ratios of their study. Figure 22 agrees with the Zhang et al (1994) study in that the mean elevation has a slightly negative correlation with the log *Pn/Lg* ratio. However, at the higher frequencies we have examined in this study, the correlations become positively sloped. Also, our study agrees with the Zhang et al (1994) study in that the best correlations are found with sediment thickness and elevation parameter and the worst correlation is with the crustal thickness.

We conclude that the best correlation appears to be with sediment thickness variations. Figure 28 shows plots of the log10 *Pn/Lg* ratio in the 8-to-16 Hz frequency band plotted versus (a) the mean sediment thickness and (b) the gradient in the sediment thickness. Strong correlations are apparent, as indicated by the large positive slopes and the small errors relative to the size of the slopes. Note that these regressions do not include the Lop Nor point, which we regard as anomalous, as shown in Figure 29. This large variance may be due to large variations in *Lg* excitation due to resonances in the sedimentary basins near WMQ. We would expect this to occur

54
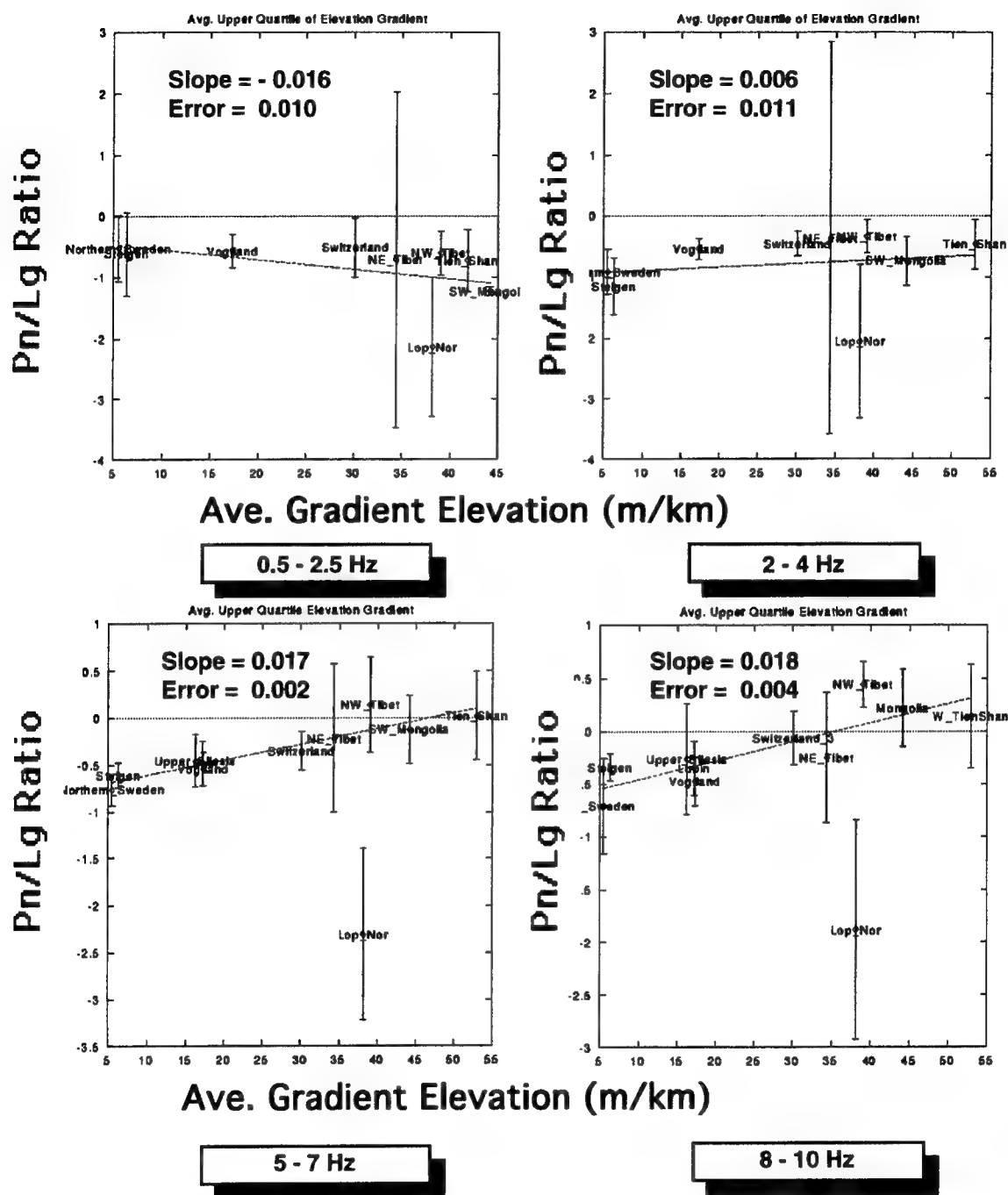
Figure 25: Correlation scatter plots of the log10 *Pn/Lg* amplitude ratios versus average upper quartile of the elevation gradient.
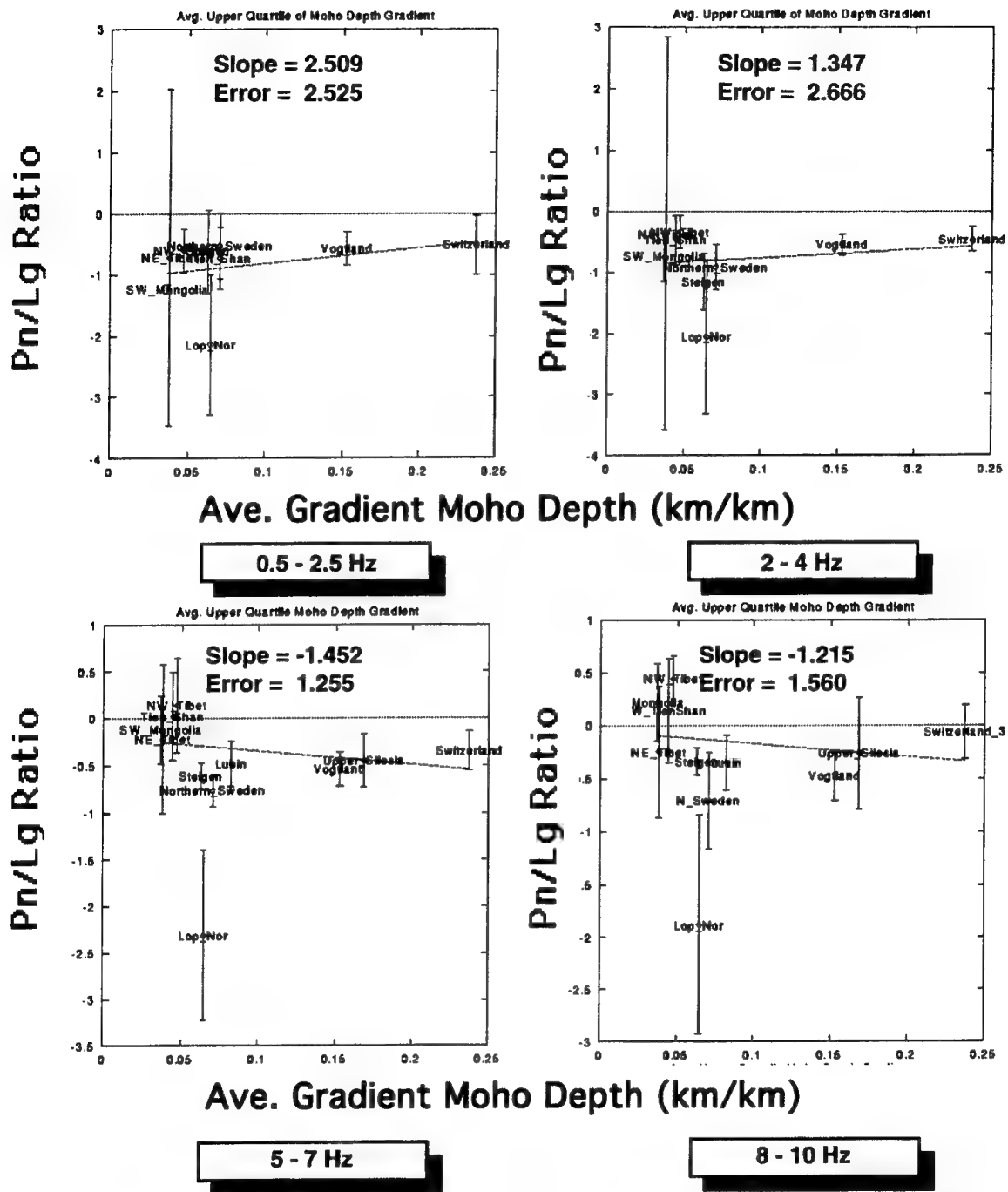
Figure 26: Correlation scatter plots of the log10 *Pn/Lg* amplitude ratios versus average upper quartile of the crustal thickness gradient along the propagation path.
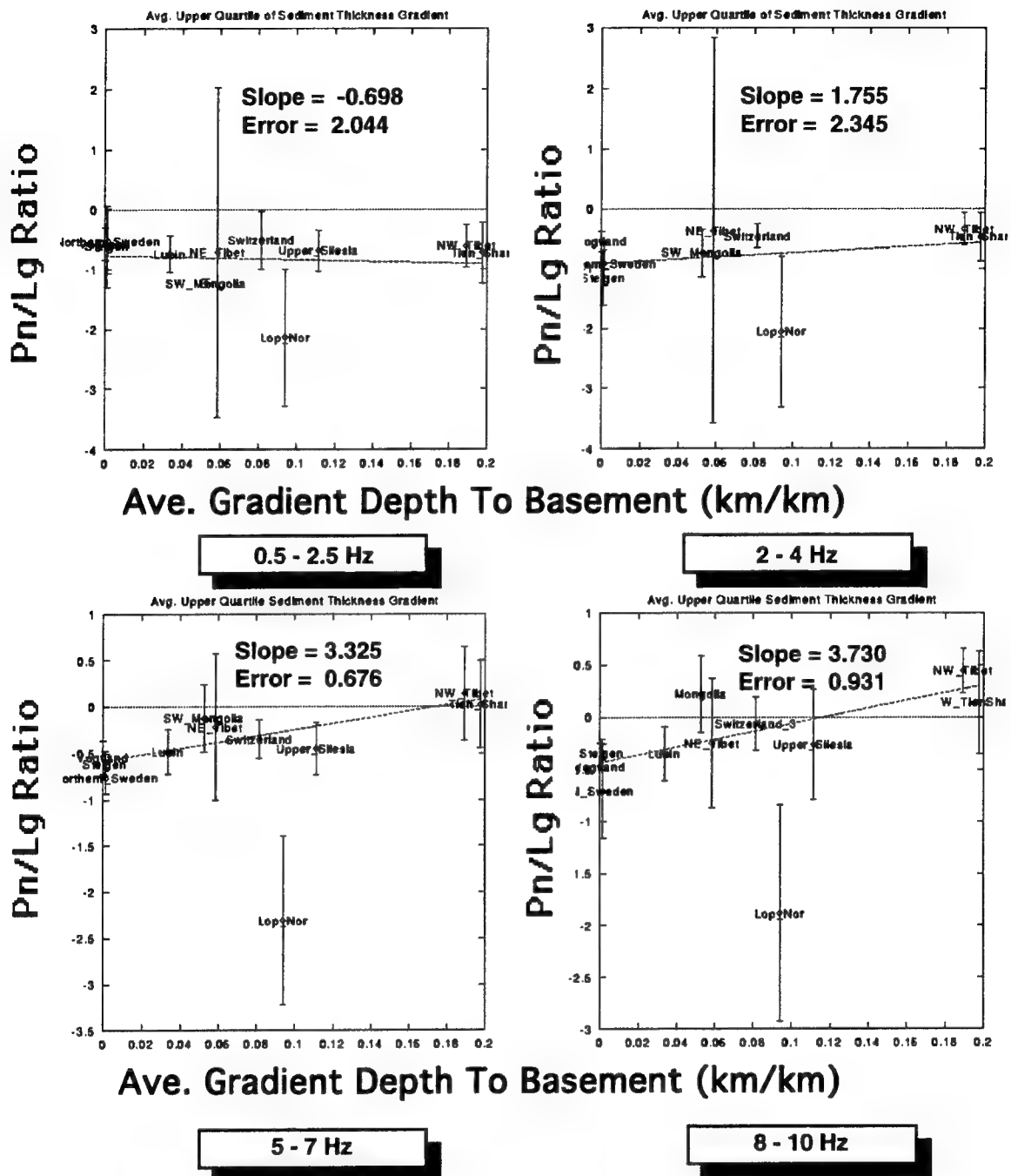
Figure 27: Correlation scatter plots of the log10 *Pn/Lg* amplitude ratios versus average upper quartile of the sediment thickness gradient along the propagation path.
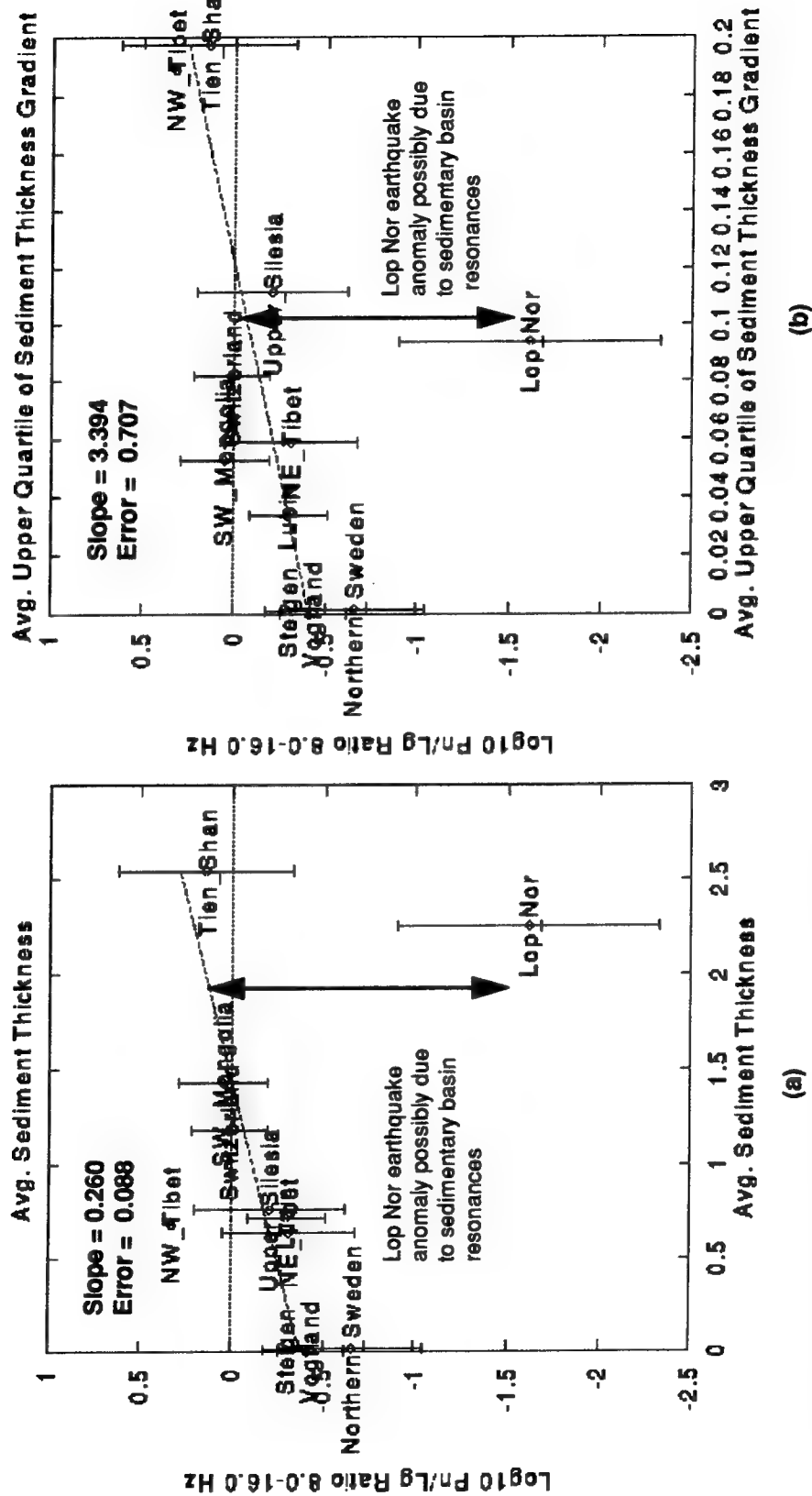
Figure 28: These plots show that correlation of 8-16 Hz Pn/Lg ratios with average crustal thickness (a) and the average of the upper quartile of the sediment thickness gradients (b). Correlation regression does not include the Lop Nor point. Anomalous values for the Lop Nor earthquakes may result from strong Lg amplitudes due to sedimentary basin resonances.

primarily in situations where either, or both the source and receiver, are in the same sedimentary basin. If the *Lg* must cross an entire basin, there may be partial blockage, of the *Lg* energy.

These plots, show that the variations in *Pn/Lg* ratios consistently depend on the tectonic type for the source region and propagation path. For example, looking at Figure 28 for the highest frequencies, the smallest ratios (i.e., largest *Lgs*) are found for propagation paths in the shield regions (Northern Sweden, Steigen, Vogtland) and the highest ratios (i.e., weakest *Lgs*) correspond to the orogenically active areas (Tien Shan, Tibet, Mongolia). The Hercynian orogenic regions of Europe (Switzerland, Upper Silesia) appear to be very similar with certain regions of China (NE Tibet, Mongolia). There is roughly a shift of about 0.8 log units between the shield and the orogenic region. This shift seems to correlate with increasing sediment thickness and thickness variations.

This approximate correlation suggests, but does not prove, a causal relation between sedimentary basin thicknesses and variations in thickness with the relative *Pn/Lg* exciation. However, this study, along with that of Zhang et al (1994), strongly suggests a correlation that may be predictive of the variations in the *Pn/Lg* ratio when one moves from a shield region to a complex tectonic region, irrespective of how it is produced. Thus, we would shift the values of discrimination thresholds by about 0.5 to 0.8 when transporting discriminants from the shield region to the orogenic region. This would not work for situations like Lop Nor, which we consider to be anomalous. However, examination of crustal cross sections would indicate if such conditions like those at Lop Nor exist. This baseline shift would apply for all distances contained within the region. Once inside the region, corrections for distance would be made using methodologies like those discussed in the last section.

5.0 CONCLUSIONS AND RECOMMENDATIONS

5.1 Summary

This study has shown that the differential effects on P and S waves of structure along the propagation path from source to receiver on P and S waves dominate the transportability of the regional P/S ratio discriminant. First, the amplitudes of Pn, Sn, and Lg attenuate at different rates; shear-wave attenuation is greater than compressional-wave attenuation, even for paths in stable shield regions. Second, crustal-structure anomalies, such as sedimentary basins, primarily block Lg waves, which propagate mainly in the upper crust, whereas Pn and Sn propagate through the mantle beneath these anomalies and are unaffected. Pn and Sn waves propagate mainly in the upper mantle lid above the mantle low velocity zone. However, Sn appears to be strongly attenuated in tectonically active regions, perhaps due to the low Q low-velocity 20 zone which is more pronounced in these regions.

Transportability of the regional P/S ratio discriminant will be of great importance in an operational CTBT monitoring system, because for most parts of the world that must be monitored, there has been no nuclear weapons testing. Identifying the "first test" requires using training data from parts of the world where nuclear testing has occurred. Thus, differences in the geology of the different regions wherein seismic events are being compared, in terms of the effects of these differences on on P and S propagation, need to be considered when using the P/S ratio for event identification.

5.2 Conclusions

In this study, we have addressed the transportability issue by comparing amplitude ratio measurements for earthquakes and explosions using data from three verydifferent tectonic regions. Based on these analyses, we arrive at the following overall conclusions:

- Distance correction curves can be derived for continental areas, assuming enough events recorded at two or more stations can found that cover a wide distance range and can be used to correct Pn/Sn and Pn/Lg ratios to a standard distance. We find exponential models seem to best fit the observed data for mine blasts and earthquakes in Scandinavia. We have assumed geometric spreading to be frequency independent and the same for P and S waves.

- Our analysis of the amplitude ratio corrections from the Sereno (1991) detection study, used by Fisk (1994) to correct Pn/Sn ratios of the Novaya

Zemlya event for distance, has a "bending down" type distance trend for Pn/Sn ratios at frequencies below 14 Hz. However, the Pn/Lg ratio curves have a cubic dependence with distance. Both of these trends to not seem to be consistent with our observations. However, with the limited data currently available and the large scatter in the observations, it is not possible to determine if either of the correction curves is best. Thus, we have incorporated both distance-correction schemes in ISEIS.

- In tectonically active regions, such as China, nuclear explosions recorded at high frequencies at all distances are fundementally P-wave sources. Lg energy is strongly attenuated at high frequency and Sn seems not to propagate at all. In shields, however, Lg can be blocked in the crust by tectonic features like sedimentary basins but high frequency Sn phases can propagate to large distances.

- The Lop Nor nuclear explosion, recorded at WMQ, can be clearly discriminated from nearby earthquakes on the basis of its high Pn/Lg ratio. Earthquakes near WMQ excite very strong Lg waves and thus produce very low Pn/Lg ratios which appear anomalous compared to more distant earthquakes. These events all occurred well inside a sedimentary basin and WMQ is near the edge of a sedimentary basin. Thus, the large Lg waves may have been generated by resonances in the soft sediments of the basin. The fact that the Lop Nor nuclear explosion is also in a sedimentary basin, but produced weak Lg waves, shows further how well the Pn/Lg ratio discriminant works.

- Examination of crustal structures for the three regions reveals that Pn/Lg ratio correlates with crustal structure parameters. Like the study of Zhang et al (1994), we find the greatest correlation with elevation and sediment thickness and their gradients. Moho depth variations have little effect on variations in Pn/Lg ratios.

- Comparing the Pn/Lg ratios of the Lop Nor nuclear explosion with those of events near ARCESS and GERESS, we find that the Lop Nor values are similar to those of mine blasts in Vogtland recorded at GERESS. ARCESS recordings of mine blasts in Scandinavia have much smaller Pn/Lg ratios than the Lop Nor nuclear explosion. Since ARCESS is in a shield region, we attribute the lower Pn/Lg ratios to the fact that Lg is less attenuated relative to Pn in the shield.

5.3   Recommendations

Further data collection and research will be required to fully assess the methodologies for transporting regional discriminants. We have only studied three different tectonic regions. Analysis of data from other tectonic regions, including regions analogous to the Scandinavian shield and tectonic orogens we have studied, need to be analyzed. Therefore, we recommend that further research with discriminant features be conducted along the following lines:

61

- Further refine the distance correction curves for *Pn/Sn* and *Pn/Lg* ratios for Scandinavia by analyzing more events. As for China, the CDSN station coverage was too sparse for us to apply the same analysis there because we were unable to find enough earthquakes in China recorded at two or more CDSN stations to derive the same curves. It may be possible to accomplish this with more stations in the region.

- The method of correlating *P/S* ratios with crustal structure parameters is promising. However, additional crustal structures would be useful. Geological and crustal structure information is now becoming available for the Middle East. When seismic data becomes available for this region in the future, similar studies there might be possible.

- As for tranporting discriminants, we believe the method of comparing events in different regions can be a very effective method of characterizing events in new regions, where there are limited training events. Perhaps very simple "baseline corrections," which do not seem to be very large, would be sufficient for correcting ratios for different regions. In general, comparing *Pn/Lg* ratios of shield regions of Scandinavia with those of tectonic active regions of China would require the latter ratios to be shifted down by as much as 0.5 to 0.8 log units relative to the shield values. These baseline shifts may be derived for different tectonic types based on extrapolations of the correlations of *Pn/Lg* ratio with crustal parameters.

REFERENCES

Anderson, J., W.E. Farrell, K. Garcia, J. Given, and H. Swanger (1990). Center for Seismic Studies Version 3 Database: Schema Reference Manual, Technical Report C90-01, Center for Seismic Studies, Arlington, VA.

Bache, T.C., S.R. Bratt, J. Wang, R.M. Fung, C. Kobryn, and J.W. Given (1990). The Intelligent Monitoring System, *Bull. Seism. Soc. Am.*, **80**, 1833-1851.

Baumgardt (1990). Investigation of Teleseismic Lg Blockage and Scattering Using Regional Arrays *Bull. Seism. Soc. Am.*, **80**, 2261-2281

Baumgardt, D.R. (1993a). Regional characterization of mine blasts, earthquakes, mine tremors, and nuclear explosions using the Intelligent Event Identification System, Final Report to ARPA, SAS-TR-94-12, ENSCO, Inc., Springfield, VA.

Baumgardt, D.R. (1993b). Seismic waveform feature and discriminaion of the December 31, 1992 Novaya Zemlya event, Paper in volume compiled by Ryall (1993).

Baumgardt, D.R. (1994). The Kiruna mine blasts of Northern Sweden: Case study of the failure of the *P/S* ratio discriminant, Topical Report submitted to ARPA, August 31, 1994.

Baumgardt, D.R. and G. Young (1990). Regional seismic waveform discriminants and case based event identification using regional arrays, *Bull. Seism. Soc. Am.*, **80**, Part B, 1874-1892.

Baumgardt, D.R. and K.A. Ziegler (1988). Spectral evidence of source multiplicity in explosions: application to regional discrimination of earthquakes and explosions. *Bull. Seism. Soc. Am.*, **78**, 1773-1795.

Baumgardt, D.R., S. Carter, M. Maxson, J. Carney, K. Ziegler, and N. Matson (1991). Design and development of the intelligent event identification system, *PL-TR-91-2298(I)*, Final Report, Volumes I, II, and III, ENSCO, Inc., Springfield, VA. Vol I: ADA248381, Vol. II: ADA248934, Vol. III: 248374

Baumgardt, D.R., J. Carney, M. Maxson, and S. Carter (1992). Evaluation of regional seismic discriminants using the Intelligent Seismic Event Identification System, Semiannual Technical Report, SAS-TR-93-38, ENSCO, Inc., Springfield, VA.

Bennett, T.J. and J.R. Murphy (1986). Analysis of seismic discrimination capabilities using regional data from western United States events, *Bull. Seism. Soc. Am.*, **76**, 1069-1086.

Bennett, T.J., B.W. Barker, K.L. McLaughlin, and J.R. Murphy (1989). Regional discrimination of quarry blasts, earthquakes, and underground nuclear explosions, Final Report, *GL-TR-89-0114*, S-Cubed, La Jolla, CA. ADA223148

Blandford, R.R. (1993). Discrimination of Earthquakes and Explosions at Regional Distances Using Complexity, *AFTAC-TR-93-044*, H.Q. Air Force Technical Applications Center, Patrick Air Force Base, FL.

Blandford, R., R. Hartenberger, and R. Naylor (1981). Regional amplitude-distance relations, discrimination and detection, *VSC-TR-81-15*, Teledyne Geotech, Alexandria, VA.

Chun, K., G.F. West, R.J. Kokoski, and C. Samson (1987). A novel technique for measuring *Lg* attenuation results from eastern Canada between 1 to 10 Hz, *Bull. Seism. Soc. Am.*, **77**, 398-419.

Chun, K., R.J. Kokoski, and G.F. West (1989). High-frequency *Pn* attenuation in the Canadian Shield, *Bull. Seism. Soc. Am.*, **79**, 1039-1053.

Dysart, P.S. and J.J. Pulli (1990). Regional seismic event classification at the NORESS array: seismological measurements and the use of trained neural networks, *Bull. Seism. Soc. Am.*, **80**, Part B, 1910-1933.

Fielding, E.J., B.L. Isacks, and M. Barazangi (1992). A geological and geophysical information system for Eurasia, *Technical Report No. 2*, Cornell University, Ithaca, New York.

Fisk, M.D. and H.L. Gray (1993). Event identification analysis of the Novaya Zemlya event on 31 December 1992 using outlier and classification likelihood ratio tests (Paper in volume compiled by A. Ryall, 1993), MRC-R-1449, Mission Research Corp., Santa Barbara, CA.

Fisk, M.D., G.L. Gray and G.D. McCartor (1993). A bootstrap generalized likelihood ratio test in discriminant analysis, in *Proceedings of the 15th Annual Seismic Research Symposium, 8-10 September 1993*, Report PL-TR-93-2160 (Eds. J.F. Lewkowicz and J.M. McPhetres), Phillips Laboratory, Hanscom AFB, MA. ADA271458

Fisk, M.D. (1994). Identification and event characterization - Getting down to the outliers, in *Proceedings of the ARPA CTBT Monitoring Technologies Conference*, 26-29 September 1994, Carmel Highland Doubletree, San Diego, CA.

Fisk, M.D., H.L. Gray, and G.D. McCartor (1994). Statistical framework of seismic event identification and preliminary assessment of seismic CTBT/NPT monitoring capability, in *Proceedings of the ARPA CTBT Monitoring Technologies Conference*, 26-29 September 1994, Carmel Highland Doubletree, San Diego, CA.

Grant, L., J. Coyne, and F. Ryall (1993). CSS Ground-Truth Database: Version 1 Handbook, *C93-05*, August 1993, Center for Seismic Studies, Arlington, VA.

Guterch, A., M. Grad, R. Materzok, and E. Perchuc (1986). Deep structure of the earth's crust in the contact zone of the Palaeozoic and Precambrian platforms in Poland (Trounquist-Teisseyre Zone), *Tectonophysics*, **128**, 251-279.

Kennett, B.L.N. (1993). The distance dependence of regional phase discriminants, *Bull. Seism. Soc. Am.*, **83**, 1155-1166.

Kim, W.Y., D.W. Simpson, and P.G. Richards (1993). Discrimination of earthquakes and explosions in the eastern United States using regional high-frequency data, *Geophys. Res. Lett.*, **20**, 1507-1510.

Kvale, A. (1976). Major features of the European Caledonides and their development, in *Europe from Crust to Core*, D.V. Ager and M. Brooks (eds.), Wiley, London.

Lynnes, C. and R. Baumstark (1991). Phase and spectral discrimination in North America, *PL-TR-91-2212 (II)*, Teledyne Geotech, Alexandria, VA. ADA246673

Molnar, P. and P. Tapponnier (1978). Active tectonics of Tibet, *J. Geophys Res.*, **83**, 5361-5375.

Murphy, J.R. and T.J. Bennett (1982). A discrimination analysis of short-period regional seismic data recorded at Tonto Forest Observatory, *Bull. Seism. Soc. Am.*, **72**, 1351-1366.

Ni, J. (1978). Contemporary tectonics in the Tien Shan region, *Earth and Planet. Sci. Lett.*, **41**, 347-354.

Ni, J. and J.E. York (1978). Late Cenozoic tectonics of the Tibetan Plateau, *J. Geophys. Res.*, **83**, 5377-5384.

Nuttli, O.W. (1981). On the attenuation of *Lg* waves in western and central Asia and their use as a discriminant between earthquakes and explosions, *Bull. Seism. Soc. Am.*, **72**, 1351-1366.

Pomeroy, P.W., W. J. Best, and T.V. McEvilly (1982). Test ban treaty verification with regional data - A review, *Bull. Seism. Soc. Am.*, **72**, S89-S129.

Riviere-Barbier, F., D. Baumgardt, and W. Rodi (1993). Using Groups of Similar Events at the Scandinavian Arrays to Identify and to Relocate Events, *Presentation at the 15th Annual Seismic Research Symposium*, 8-10 September 1993, Vail, CO. PL-TR-93-2160, ADA271458

Ryall, A. (1993). Seismic Identification Issues and The Novaya Zemlya Event of 31 December 1992, *Presentation at the 15th Annual Seismic Research Symposium*, 8-10 September 1993, Vail, CO. PL-TR-93-2160, ADA271458

Sereno, T.J. (1991). Simulation of the detection and location capability of regional seismic networks in the Soviet Union, Final Report, SAIC-91/1061, SAIC, San Diego, CA.

Taylor, S.R., N.W. Sherman, and M.D. Denny (1988). Spectral discrimination between NTS explosions and western United States earthquakes at regional distances, *Bull. Seism. Soc. Am.*, **78**, 1563-1579.

Taylor, S.R., M.D. Denny, E.S. Vergino, and R.E. Glaser (1989). Regional discrimination between NTS explosion and western United States earthquakes, *Bull. Seism. Soc. Am.*, **79**, 1142-1176.

Tapponnier, P. and P. Molnar (1977). Active faulting and tectonics in China, *J. Geophys Res.*, **82**, 2905-2930.

Tapponnier, P. and P. Molnar (1979). Active faulting and cenozoic tectonica of the Teien Shan, Mongolia, and Baykal regions, *J. Geophys. Res.*, **84**, 3425-3459.

Terman, M.J. and C.C. Woo (1967). Atlas of Asia and Eastern Europe to support detection of underground nuclear testing, Vol. II, Tectonics, China and Mongolia, Prepared for ARPA by USGS.

Watson, J. (1976). *Eo_Europa:* the evolution of a craton, in *Euorpe from Crust to Core*, D.V. Ager and M. Brooks (eds.), Wiley, London.

Woods, B.B., S. Kedar, and D.V. Helmberger (1993). M_L-M_0 as a regional discriminant, *Bull. Seism. Soc. Am.*, **83**, 1167-1183.

Wuster, J. (1993). Discrimination of chemical explosions and earthquakes in central Europe - a case study, *Bull. Seism. Soc. Am.*, **83**, 1184-1212.

Zhang, T. and T. Lay (1994a). Analysis of short-period regional phase path effects associated with topography in Eurasia, *Bull. Seism. Soc. Am.*, **84**, 119-132.

Zhang, T. and T. Lay (1994b). Effects of crustal structure under the Barents and Kara Seas on short-period regional wave propgation for Novaya Zemlya explosions: empirical relations, *Bull. Seism. Soc. Am.*, **84**, 1132-1147.

Zhang, T., S.Y. Schwartz, and T. Lay (1994). Multivariate analysis of waveguide effects on short-period regional wave propagation in Eurasia and its application in seismic discrimination, *J. Geophys. Res.*, **99**, 21929-21946.

Prof. Thomas Ahrens
Seismological Lab, 252-21
Division of Geological & Planetary Sciences
California Institute of Technology
Pasadena, CA 91125

Prof. Keiiti Aki
Center for Earth Sciences
University of Southern California
University Park
Los Angeles, CA 90089-0741

Prof. Shelton Alexander
Geosciences Department
403 Deike Building
The Pennsylvania State University
University Park, PA 16802

Dr. Thomas C. Bache, Jr.
Science Applications Int'l Corp.
10260 Campus Point Drive
San Diego, CA 92121 (2 copies)

Prof. Muawia Barazangi
Cornell University
Institute for the Study of the Continent
3126 SNEE Hall
Ithaca, NY 14853

Dr. Douglas R. Baumgardt
ENSCO, Inc
5400 Port Royal Road
Springfield, VA 22151-2388

Dr. T.J. Bennett
S-CUBED
A Division of Maxwell Laboratories
11800 Sunrise Valley Drive, Suite 1212
Reston, VA 22091

Dr. Robert Blandford
AFTAC/TT, Center for Seismic Studies
1300 North 17th Street
Suite 1450
Arlington, VA 22209-2308

Dr. Steven Bratt
ARPA/NMRO
3701 North Fairfax Drive
Arlington, VA 22203-1714

Dale Breding
U.S. Department of Energy
Recipient, IS-20, GA-033
Office of Arms Control
Washington, DC 20585

Dr. Jerry Carter
Center for Seismic Studies
1300 North 17th Street
Suite 1450
Arlington, VA 22209-2308

Mr Robert Cockerham
Arms Control & Disarmament Agency
320 21st Street North West
Room 5741
Washington, DC 20451,

Dr. Zoltan Der
ENSCO, Inc.
5400 Port Royal Road
Springfield, VA 22151-2388

Dr. Stanley K. Dickinson
AFOSR/NM
110 Duncan Avenue
Suite B115
Bolling AFB, DC

Dr Petr Firbas
Institute of Physics of the Earth
Masaryk University Brno
Jecna 29a
612 46 Brno, Czech Republic

Dr. Mark D. Fisk
Mission Research Corporation
735 State Street
P.O. Drawer 719
Santa Barbara, CA 93102

Dr. Cliff Frolich
Institute of Geophysics
8701 North Mopac
Austin, TX 78759

Dr. Holly Given
IGPP, A-025
Scripps Institute of Oceanography
University of California, San Diego
La Jolla, CA 92093

Dr. Jeffrey W. Given
SAIC
10260 Campus Point Drive
San Diego, CA 92121

Dr. Dale Glover
Defense Intelligence Agency
ATTN: ODT-1B
Washington, DC 20301

1

Dan N. Hagedon
Pacific Northwest Laboratories
Battelle Boulevard
Richland, WA 99352

Dr. James Hannon
Lawrence Livermore National Laboratory
P.O. Box 808, L-205
Livermore, CA 94550

Dr. Roger Hansen
University of Colorado, JSPC
Campus Box 583
Boulder, CO 80309

Prof. David G. Harkrider
Division of Geological & Planetary Sciences
California Institute of Technology
Pasadena, CA 91125

Prof. Danny Harvey
University of Colorado, JSPC
Campus Box 583
Boulder, CO 80309

Prof. Donald V. Helmberger
Division of Geological & Planetary Sciences
California Institute of Technology
Pasadena, CA 91125

Prof. Eugene Herrin
Geophysical Laboratory
Southern Methodist University
Dallas, TX 75275

Prof. Robert B. Herrmann
Department of Earth & Atmospheric Sciences
St. Louis University
St. Louis, MO 63156

Prof. Lane R. Johnson
Seismographic Station
University of California
Berkeley, CA 94720

Prof. Thomas H. Jordan
Department of Earth, Atmospheric &
 Planetary Sciences
Massachusetts Institute of Technology
Cambridge, MA 02139

Robert C. Kemerait
ENSCO, Inc.
445 Pineda Court
Melbourne, FL 32940

U.S. Dept of Energy
Max Koontz, NN-20, GA-033
Office of Research and Develop.
1000 Independence Avenue
Washington, DC 20585

Dr. Richard LaCoss
MIT Lincoln Laboratory, M-200B
P.O. Box 73
Lexington, MA 02173-0073

Prof. Charles A. Langston
Geosciences Department
403 Deike Building
The Pennsylvania State University
University Park, PA 16802

Jim Lawson, Chief Geophysicist
Oklahoma Geological Survey
Oklahoma Geophysical Observatory
P.O. Box 8
Leonard, OK 74043-0008

Prof. Thorne Lay
Institute of Tectonics
Earth Science Board
University of California, Santa Cruz
Santa Cruz, CA 95064

Dr. William Leith
U.S. Geological Survey
Mail Stop 928
Reston, VA 22092

Mr. James F. Lewkowicz
Phillips Laboratory/GPE
29 Randolph Road
Hanscom AFB, MA 01731-3010(2 copies)

Dr. Gary McCartor
Department of Physics
Southern Methodist University
Dallas, TX 75275

Prof. Thomas V. McEvilly
Seismographic Station
University of California
Berkeley, CA 94720

2

Dr. Keith L. McLaughlin
S-CUBED
A Division of Maxwell Laboratory
P.O. Box 1620
La Jolla, CA 92038-1620

Mr. Wilmer Rivers
Multimax Inc.
1441 McCormick Drive
Landover, MD 20785

Prof. Bernard Minster
IGPP, A-025
Scripps Institute of Oceanography
University of California, San Diego
La Jolla, CA 92093

Dr. Alan S. Ryall, Jr.
Lawrence Livermore National Laboratory
L-025
P.O. Box 808
Livermore, CA 94550

Prof. Brian J. Mitchell
Department of Earth & Atmospheric Sciences
St. Louis University
St. Louis, MO 63156

Dr.Chandan K. Saikia
Woodward Clyde- Consultants
566 El Dorado Street
Pasadena, CA 91101

Mr. Jack Murphy
S-CUBED
A Division of Maxwell Laboratory
11800 Sunrise Valley Drive, Suite 1212
Reston, VA 22091 (2 Copies)

Mr. Dogan Seber
Cornell University
Inst. for the Study of the Continent
3130 SNEE Hall
Ithaca, NY 14853-1504

Dr. Keith K. Nakanishi
Lawrence Livermore National Laboratory
L-025
P.O. Box 808
Livermore, CA 94550

Secretary of the Air Force
(SAFRD)
Washington, DC 20330

Prof. John A. Orcutt
IGPP, A-025
Scripps Institute of Oceanography
University of California, San Diego
La Jolla, CA 92093

Office of the Secretary of Defense
DDR&E
Washington, DC 20330

Dr. Howard Patton
Lawrence Livermore National Laboratory
L-025
P.O. Box 808
Livermore, CA 94550

Thomas J. Sereno, Jr.
Science Application Int'l Corp.
10260 Campus Point Drive
San Diego, CA 92121

Dr. Frank Pilotte
HQ AFTAC/TT
1030 South Highway A1A
Patrick AFB, FL 32925-3002

Dr. Michael Shore
Defense Nuclear Agency/SPSS
6801 Telegraph Road
Alexandria, VA 22310

Dr. Jay J. Pulli
Radix Systems, Inc.
201 Perry Parkway
Gaithersburg, MD 20877

Prof. David G. Simpson
IRIS, Inc.
1616 North Fort Myer Drive
Suite 1050
Arlington, VA 22209

Prof. Paul G. Richards
Lamont-Doherty Earth Observatory
 of Columbia University
Palisades, NY 10964

Dr. Jeffrey Stevens
S-CUBED
A Division of Maxwell Laboratory
P.O. Box 1620
La Jolla, CA 92038-1620

Prof. Brian Stump
Los Alamos National Laboratory
EES-3
Mail Stop C-335
Los Alamos, NM 87545

Prof. Tuncay Taymaz
Istanbul Technical University
Dept. of Geophysical Engineering
Mining Faculty
Maslak-80626, Istanbul Turkey

Prof. M. Nafi Toksoz
Earth Resources Lab
Massachusetts Institute of Technology
42 Carleton Street
Cambridge, MA 02142

Dr. Larry Turnbull
CIA-OSWR/NED
Washington, DC 20505

Dr. Karl Veith
EG&G
5211 Auth Road
Suite 240
Suitland, MD 20746

Prof. Terry C. Wallace
Department of Geosciences
Building #77
University of Arizona
Tuscon, AZ 85721

Dr. William Wortman
Mission Research Corporation
8560 Cinderbed Road
Suite 700
Newington, VA 22122

ARPA, OASB/Library
3701 North Fairfax Drive
Arlington, VA 22203-1714

HQ DNA
ATTN: Technical Library
Washington, DC 20305

Defense Technical Information Center
Cameron Station
Alexandria, VA 22314 (2 Copies)

TACTEC
Battelle Memorial Institute
505 King Avenue
Columbus, OH 43201 (Final Report)

Phillips Laboratory
ATTN: GPE
29 Randolph Road
Hanscom AFB, MA 01731-3010

Phillips Laboratory
ATTN: TSML
5 Wright Street
Hanscom AFB, MA 01731-3004

Phillips Laboratory
ATTN: PL/SUL
3550 Aberdeen Ave SE
Kirtland, NM 87117-5776 (2 copies)

Dr. Michel Campillo
Observatoire de Grenoble
I.R.I.G.M.-B.P. 53
38041 Grenoble, FRANCE

Dr. Kin Yip Chun
Geophysics Division
Physics Department
University of Toronto
Ontario, CANADA

Prof. Hans-Peter Harjes
Institute for Geophysic
Ruhr University/Bochum
P.O. Box 102148
4630 Bochum 1, GERMANY

Prof. Eystein Husebye
NTNF/NORSAR
P.O. Box 51
N-2007 Kjeller, NORWAY

David Jepsen
Acting Head, Nuclear Monitoring Section
Bureau of Mineral Resources
Geology and Geophysics
G.P.O. Box 378, Canberra, AUSTRALIA

Ms. Eva Johannisson
Senior Research Officer
FOA
S-172 90 Sundbyberg, SWEDEN

4

Dr. Peter Marshall
Procurement Executive
Ministry of Defense
Blacknest, Brimpton
Reading FG7-FRS, UNITED KINGDOM

Dr. Bernard Massinon, Dr. Pierre Mechler
Societe Radiomana
27 rue Claude Bernard
75005 Paris, FRANCE (2 Copies)

Dr. Svein Mykkeltveit
NTNT/NORSAR
P.O. Box 51
N-2007 Kjeller, NORWAY (3 Copies)

Dr. Jorg Schlittenhardt
Federal Institute for Geosciences & Nat'l Res.
Postfach 510153
D-30631 Hannover , GERMANY

Dr. Johannes Schweitzer
Institute of Geophysics
Ruhr University/Bochum
P.O. Box 1102148
4360 Bochum 1, GERMANY

Trust & Verify
VERTIC
Carrara House
20 Embankment Place
London WC2N 6NN, ENGLAND